1 Executive summary

The aim of MultiHy was to develop and test a framework for simulation of hydrogen embrittlement (HE) in real industrial problems. The most reliable and transferrable approach to modelling HE is to develop accurate descriptions of H diffusion and trapping. Since H diffusion and trapping are influenced by a variety of factors from the atomistic (e.g. crystal structure and defects) to the macro scale (e.g. stress and temperature gradients), this necessitated a true multiscale modelling framework.

A key aspect of the project was the use of results of atomistic simulations for H interactions with crystal defects in finite element (FE) models that can be scaled up to the component level. Critical to achieving this goal was overcoming the temporal and spatial differences between atomistic and FE modelling methods. This has been achieved by deriving the input parameters for the FE models from atomistic modelling results using kinetic Monte Carlo (kMC) simulations. An extensive program of experiments using specially-fabricated model materials was also carried out in order to provide data to validate or supplement the models.

The models were applied to three industrial case studies involving HE:

- **CS1:** Delayed H-assisted cracking of pulse plated (PP) Ni combustion chambers for the Ariane 5 satellite launcher.
- **CS2:** HE of advanced high strength steel (AHSS) for automobile “body-in-white” components.
- **CS3:** H-assisted rolling contact fatigue (HA-RCF) of large sized bearings (LSBs) in offshore wind turbines.

The primary focus of CS1 has been the evaluation of the influence of grain boundaries on H diffusion in PP-Ni. Grain boundaries may act as preferential pathways for H diffusion in nanocrystalline materials such as PP-Ni. We have used atomistic calculations to evaluate the diffusivity of H along various types of grain boundaries in Ni. The results were applied in kMC and FE simulations based on real microstructural data. The FE models then were scaled-up such as to evaluate the influence of grain structure on the damage tolerance of PP-Ni components.

Work in CS2 and CS3 has generally sought to evaluate whether HE of steels may be mitigated by the presence of TiC, NbC, and VC particles, respectively, in the microstructure. Such particles have long been known to behave as strong trap sites. Atomistic calculations of H trapping by TiC and VC particles were performed and the results used in FE simulations of H diffusion at the continuum and component levels. An exhaustive experimental program aimed at evaluating the influence of carbides, especially TiC, on H diffusion and trapping in steels has also been carried out.

Ultimately, the outcomes of the project will assist the industrial partners in making more informed decisions regarding the selection of materials and processing parameters to minimise the risk of failure due to HE.

2 Summary description of project context and objectives

2.1 Background information

Hydrogen embrittlement (HE) is an insidious failure mode that affects all structural metals to some extent. Given the ubiquity of H in service environments, this represents a very serious threat to the integrity of structural components across all industries. Despite having been studied extensively since the 1930s, there is still considerable debate regarding the mechanisms for HE, in particular regarding the role of H in damage processes. Several mechanisms for H-assisted damage have been proposed. Some of these are supported by considerable experimental and theoretical evidence, though there exist various doubts regarding the validity of each. This confusion is compounded by the dependence of the predominant mechanism on a number of factors, including microstructure and mechanical/environmental conditions. Consequently, in most cases the predominant H-assisted damage mechanism is uncertain. This is especially true for real engineering materials with complex microstructures under real operating conditions.

A common factor in all H-assisted damage mechanisms is the crucial role of H diffusion and trapping. In many cases it is possible to characterise the lifetime of a susceptible component in the presence of H by the time taken for H to accumulate in sufficient quantities at the fracture site. This necessitates a profound understanding of the interactions of H with microstructural features and defects at the atomic through to the macro scale. Such interactions are more amenable to evaluation using numerical and experimental techniques than the influence of H on damage and fracture processes. Thus, a pragmatic approach to modelling of industrial problems involving HE should focus primarily on developing a detailed understanding of H diffusion and trapping in real material microstructures under service conditions. This can be used to evaluate the critical local conditions causing H-assisted damage and the key microstructural features affecting H transport to the fracture site.

H transport and, therefore, HE susceptibility are profoundly affected by the strength and distribution of trap sites. Trap sites may include point defects and their complexes, solute atoms, second phase particles, grain or phase interfaces, twin boundaries, and dislocations. The influence of traps on H transport depends on their binding energy and the boundary conditions, i.e. the source of H. The binding energies of traps can be evaluated by numerical modelling on the atomistic level and, to some extent, by experimental techniques such as thermal desorption spectroscopy (TDS) and permeation testing. There is a limited body of literature on the determination of diffusion barriers for atomic complexes, crystallographic defects and simple microstructural features using numerical simulations; however, a complete database of diffusion barriers that are encountered in real material microstructures is far off.

2.2 Scope and objectives of the project

The primary objective of MultiHy was to develop a framework that could be used to evaluate the HE susceptibility of components made from complex engineering materials under realistic service conditions. Given the inherent uncertainty regarding

the predominant H-assisted damage mechanisms, the project would focus on developing of accurate descriptions of H diffusion. However, since H diffusion is affected by a variety of factors from the atomistic (e.g. crystal structure and defects) to the macro scale (e.g. stress and temperature gradients), this necessitated the development of a true multiscale modelling framework. Thus, critical to achieving this objective is the extraction and propagation of information pertaining to critical microstructural features and defects from the atomistic level to the component scale.

At the atomistic level, the project would make extensive use of quantum mechanical (i.e. first-principals or ab-initio) modelling methods as well as simplified empirical potentials to evaluate the binding energies and energy barriers for H diffusion in bulk phases and near microstructural features and defects. It is important to note, however, that all such methods have some intrinsic drawbacks. First-principles calculations may be used to accurately determine the energetics of H in bulk crystals and for the simplest point defects. However, such calculations are computationally expensive. This prohibits their application to extended defects such as dislocations and interfaces involving large numbers of atoms and complicated boundary conditions. H interactions with such defects must be treated using semi-empirical schemes such as those based on the embedded atom method (EAM). However, such schemes are less accurate and reliable than first-principals calculations, depending on the type of interatomic potential used.

One of the most severe shortcomings of all atomistic simulations is their temporal aspect. Atomistic simulations are able to follow the dynamic development of a system only for very short times (of the order of nanoseconds). This prohibits their application to simulation of long range diffusion over extended time scales. In MultiHy, this limitation has been overcome through the use of kinetic Monte Carlo. This involves statistical averaging of the movement of H atoms based on a pre-defined map of the potential energy surface (PES), i.e. the energies of individual states and the energy barriers between them, which can be furnished by atomistic calculations. Mesoscopic kMC simulations may be used to calculate, for example, the diffusivity of H through a crystal environment containing different combinations of traps, which is an essential input for FE simulations.

Continuum descriptions of H diffusion and trapping are well established and there are numerous examples in the literature of their implementation at the macro scale, e.g. using finite element (FE) methods. FE models are virtually unlimited in their applicability to different time and length scales. This makes them ideally suited to simulations involving components with complex geometries under dynamic boundary conditions. However, the application of FE models to the prediction of the damage tolerance of components often requires the resolution of features at both the micro (e.g. small cracks) and macro (e.g. component boundaries) scales. This sometimes necessitates the use of advanced discretisation methods to enable the transfer of information between scales.

In lieu of any theoretical treatment of H-assisted damage mechanisms, the models would be related to materials reliability and lifetime assessment by determining the local conditions (in terms of H concentration and stress/strain condition) at the point

and instant of fracture. The local conditions would be determined by applying the numerical models to controlled experimental measurements of the mechanical thresholds in the presence of hydrogen, e.g. tensile tests of H-charged samples. They would then be incorporated into the numerical models at the component level as the fracture criteria, thereby enabling evaluation of the damage tolerance of the component.

The assessment of degradation and reliability of materials and components would also be enhanced by the use of boundary conditions based on measurements taken in-service or during component laboratory tests. A significant part of the project was devoted to the collection and analysis of data pertaining to the process or service conditions causing HE. This data included process parameters and operating conditions as well as material characteristics (e.g. concentration and distribution of absorbed H and residual stresses) after as a result of processing or service.

An extensive program of experiments using specially-fabricated model materials was also carried out in order to provide data to validate or supplement the models. In addition to the tensile tests used to evaluate the fracture criteria, thermal desorption spectroscopy (TDS) and electrochemical permeation tests were used to evaluate the binding energies if traps. Detailed microstructural characterisation was also performed for all model materials in order to identify critical trap sites and provide the microstructural data necessary for building the numerical models.

2.3 Application to industrial problems

The models have been applied to three industrial case studies involving HE:

CS1 - Delayed H-assisted cracking in pulse-plated Ni

Pulse-plate (PP) Ni is used for the construction of critical components of space vehicles such as the Ariane 5 satellite launcher. The PP process offers a number of distinct advantages over conventional electrodeposition processes, including lower cost and improved mechanical properties. This enables the fabrication of thinner (and lighter) components, thereby improving the fuel efficiency and payload capacity of the vehicle. Experience at Airbus Defence and Space has shown that, depending on the plating parameters used, PP-Ni components may fail due to delayed H-assisted cracking, with the source of H being the deposition process itself. Though this does not pose an immediate structural integrity problem, the company aims to further optimise its production process by developing a better understanding of the influence of microstructure and process parameters on the susceptibility of PP-Ni to delayed cracking. Due to its unique microstructure, it was assumed that grain boundaries play an important role in the diffusion of H in PP-Ni. Thus, the main focus of CS1 was the evaluation of H diffusion along grain boundaries and the influence of different grain structures on the bulk diffusion rate.

CS2 - HE of advanced high strength steels for automotive applications

There is growing interest in the use of advanced high strength steel (AHSS) grades for structural automobile components due to their combination of high specific strength and ductility. There is, however, a perception that AHSS grades are

susceptible to HE, with the H being absorbed as a result of manufacturing processes or during the product life cycle. There is an urgent need to better understand the influence of microstructure on the susceptibility of AHSS grades and to reduce their susceptibility through microstructural modification. One possible means of achieving this is by reducing the rate with which H accumulates at crack initiation sites by introducing strong, innocuous trap sites to the microstructure. TiC and NbC particles are have long been known to behave as strong trap sites. Thus, the primary focus of CS2 was the evaluation of the H trapping characteristics of TiC and NbC particles and their influence on the HE susceptibility of AHSS grades.

CS3 - H-assisted rolling contact fatigue of wind turbine bearings

H-assisted rolling contact fatigue (HA-RCF) is an ongoing problem that affects bearings in a diverse range of applications. H may be generated in bearings in a tribo-chemical degradation reaction of the lubricant. This H may be absorbed by the bearing material, where it accelerates the damage processes, ultimately resulting in premature failure of the bearing. This is a particular problem in “large size bearings” (LSBs) using in offshore wind turbines. The long maintenance intervals for offshore turbines necessitate the use of long-life lubricants, which contain a high number of additives, making them more prone to decomposition and H generation. This increases the risk of failure due to HA-RCF. Thus, there is strong demand for modelling tools that can be used to predict the influence of H on the service life of wind turbine bearings and to identify suitable countermeasures, e.g. microstructural modification of the bearing material. Bearing steels containing VC particles, which have strong trapping characteristics, have already been shown to have a high resistance to HA-RCF. CS3 has, therefore, focused on evaluating the trapping characteristics of VC particles and their influence on bearing lifetime.

2.4 Project outcomes and their impact and use

The project has resulted in the development of advanced multiscale models that are capable of predicting the susceptibility of materials and components to HE in the context of three industrial case studies. In each case study, we have developed FE models for the evaluation of the influence of H on the damage tolerance of materials and components. These models have been informed by atomistic and kMC simulations, microstructural data, experimental measurements and in-service data collection. These tools will assist companies in making more informed decisions regarding the selection of materials and processing parameters to minimise the risk of failure due to HE.

3 Description of main S&T results/foreground

3.1 WP1: Microstructural characterisation and micromechanical testing

3.1.1 Scope and objectives

The aim of WP1 was to collect detailed information regarding the microstructures of the model materials that are the focus of MultiHy. This information would form the

basis for the development of numerical models for H-microstructure interactions and would also be correlated with experimental measurements in order to evaluate the H diffusion and trapping characteristics of certain microstructural features and defects. A wide range of methods have been employed in order to accurately characterise the material microstructures. Optical metallography and scanning electron microscopy (SEM) were used to develop a general understanding of the materials and identify key aspects of their microstructures that are likely to affect hydrogen diffusion. More detailed analysis of these key aspects has been performed using transmission electron microscopy (TEM). We have also made extensive use of electron backscatter diffraction (EBSD) and X-ray diffraction (XRD) to characterise the crystallography of the materials.
Micromechanical testing was also carried out in order to evaluate the influence of H on the mechanical properties of the materials in the nanometre range, where they can be more-easily related to the outcomes of the atomistic and kMC calculations in WP4 and WP5 respectively. This has been achieved through nanoindentation and micro-compression of focused ion beam (FIB) prepared micropillars in combination with in-situ electrochemical H charging.

3.1.2 Summary of results

WP1.1: Fabrication of model materials and components

CS1

The model materials in CS1 were different varieties of pulse-plated (PP) Ni. This material is used in the fabrication of rocket combustion chambers for the Ariane satellite launcher (see Figure 1).

Figure 1: Vulcain 2 (A) and Vinci (B) rocket engines

PP-Ni is produced via an electroplating process. This differs from conventional direct current (DC) electroplating processes in that it employs an alternating current which

results in a higher quality deposition. During manufacture of the combustion chambers, a Ni layer of thickness up to 20 mm is deposited onto a copper substrate using the PP-process. The microstructure of the PP-Ni is greatly dependent on the plating parameters and electrolyte used.

Three types of PP-Ni were selected for evaluation in order to evaluate the influences of plating parameters on susceptibility to delayed H-assisted cracking. These are referred to as “common old”, “common new”, and “intermediate”. Common old and common new are produced using the same parameters but a different electrolyte; common old is susceptible to delayed H-assisted cracking whereas common new did not show any susceptibility so far. Intermediate is produced using the same electrolyte as common new but different parameters; it has so far not exhibited delayed H-assisted cracking during its short application time.

CS2

A primary objective of CS2 was the evaluation of titanium-carbide (TiC) and niobium-carbide (NbC) particles as a means of mitigating hydrogen embrittlement of advanced high strength steel (AHSS). Two groups of steels with similar compositions, referred to as the “VAS-concept” and “TKSE-concept”, were developed for this project (see Figure 2). Small quantities of titanium and niobium were added to the VAS-concept and TKSE-concept steels, respectively, with the aim of precipitating TiC and NbC particles. Each group was annealed into two strength classes (with ultimate tensile strengths of approximately 1200 and 1400 MPa) and four different AHSS grades, namely, martensitic (M), tempered martensitic (TM), complex phase (MTM) and dual phase (DP, M05, M04, TM09). This resulted in total of eight different grades, each with and without Ti or Nb additions. The steels were rolled into sheets of thickness 1 or 1.5 mm, and subsequently specimens were machined from the sheets for experiments in WP2.

The fabrication of materials in CS2 began immediately in the beginning of the project. Processing of materials, including casting and rolling, was conducted by VAS with the exception of the Ti-containing TKSE-concept steels.

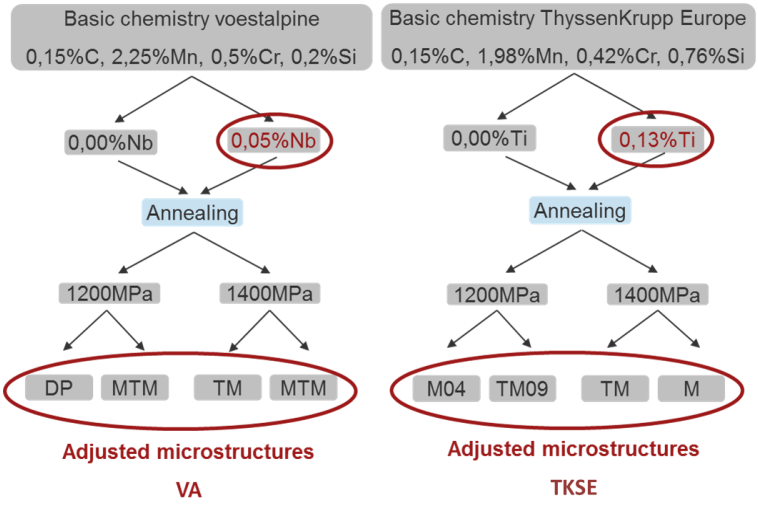

Figure 2: Basic chemical composition and adjusted microstructures.

The two basic compositions were melted in an open hearth induction furnace and cast into lab-scaled size ingots (Figure 3). The exact compositions of the two groups are given in Table 1. The compositions are similar to those of industrial high-strength materials with tensile strengths of 1000 MPa and higher, with the exception that these basic compositions contain no micro-alloying elements. Aside from their Nb and Ti concentrations, the two basic compositions differed only in their Mn and Si contents which affect the thermodynamic properties and require a different processing route.

Table 1: Chemistry for all lab heats (in mass-%).

	C	Si	Mn	P	S	Al	Cr	Ni	Mo	Cu	V	Nb	B	Ti	N
VAS concept without Nb	0,158	0,20	2,29	0,0047	0,0050	0,044	0,48	0,009	0,003	0,015	0,002	<0,002	<0,0002	<0,001	0,0045
VAS concept with Nb	0,156	0,20	2,30	0,0047	0,0032	0,034	0,49	0,011	0,003	0,016	0,002	0,048	<0,0002	<0,001	0,0049
TKSE concept without Ti	0,152	0,72	1,91	0,0051	0,0062	0,030	0,43	0,009	0,005	0,016	0,002	<0,002	0,0004	<0,001	0,0044
TKSE concept with Ti	0,152	0,73	1,93	0,0054	0,0037	0,035	0,43	0,011	0,006	0,017	0,006	0,002	0,0030	0,089	0,0048

Figure 3: Nb-containing ingot after casting (~90kg).

The ingots were machined and hot rolled in order to produce strips with a thickness of about 4 mm (Figure 4) for cold rolling. Prior to cold rolling, the scale was removed from the sheets by sand blasting (Figure 5).

Figure 4: Material in hot rolled condition.

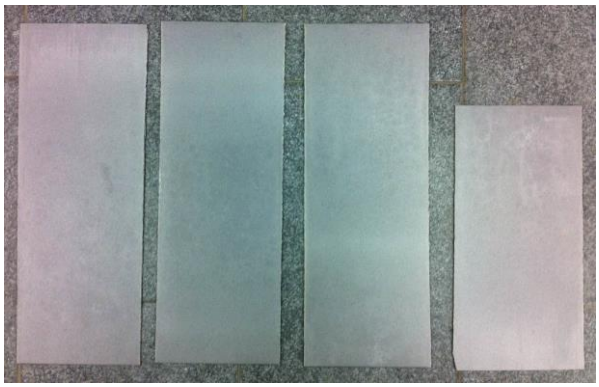

Figure 5: Sand blasted material before cold rolling.

In the cold-rolling step the thickness of the hot strip was reduced to 1 or 1.5 mm in several passes (Figure 6). Cold-rolling of the hot strips produced from the Ti-containing ingots was performed by TKSE while cold-rolling of the hot strips produced from the other ingots was performed by VAS.

Figure 6: Finishing of cold rolling process, material in hardened condition.

Annealing of the VAS-concept and TKSE-concept cold-rolled sheets was carried out separately at VAS and TKSE respectively. After cold-rolling, annealing specimens were prepared from the VAS-concept materials and clamped in the annealing equipment. Various cooling and reheating protocols were then applied in order to produce the required microstructures (Figure 7).

The annealing procedure carried out at TKSE was similar to that used at VAS. Prior annealing, the cold-rolled strips were machined into sheets as required by the annealing simulator. The specimens were then annealed in the simulator using resistive heating, air pressure cooling and, if necessary, water quenching (Figure 8).

Since the annealed specimens were covered by an oxide layer, further processing was required in order to remove these layers. The specimens were often warped due to the rapid cooling step.

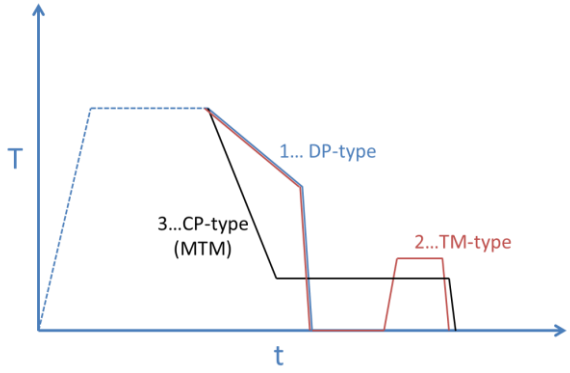

Figure 7: Annealing cycles for VAS concept steels.

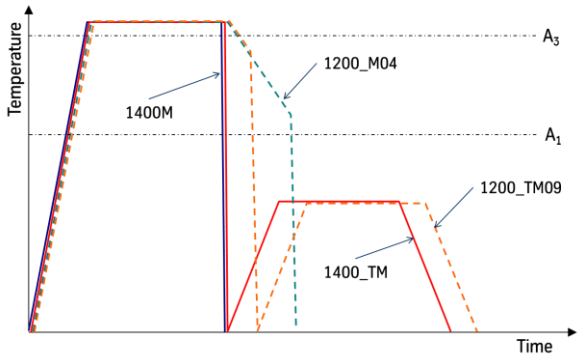

Figure 8: Annealing cycles for TKSE concept steels.

WP1.2: Microstructural characterisation

CS1

Figure 9 shows optical micrographs of the three model materials. All PP-Ni materials had a characteristic dendritic grain structure. In the case of “common old” and “common new” the dendrites were clustered in elongated “columns”, which were oriented parallel with the growth direction. These columns were larger for “common new” than for “common old”. Columns were not discernible in the “intermediate” material.

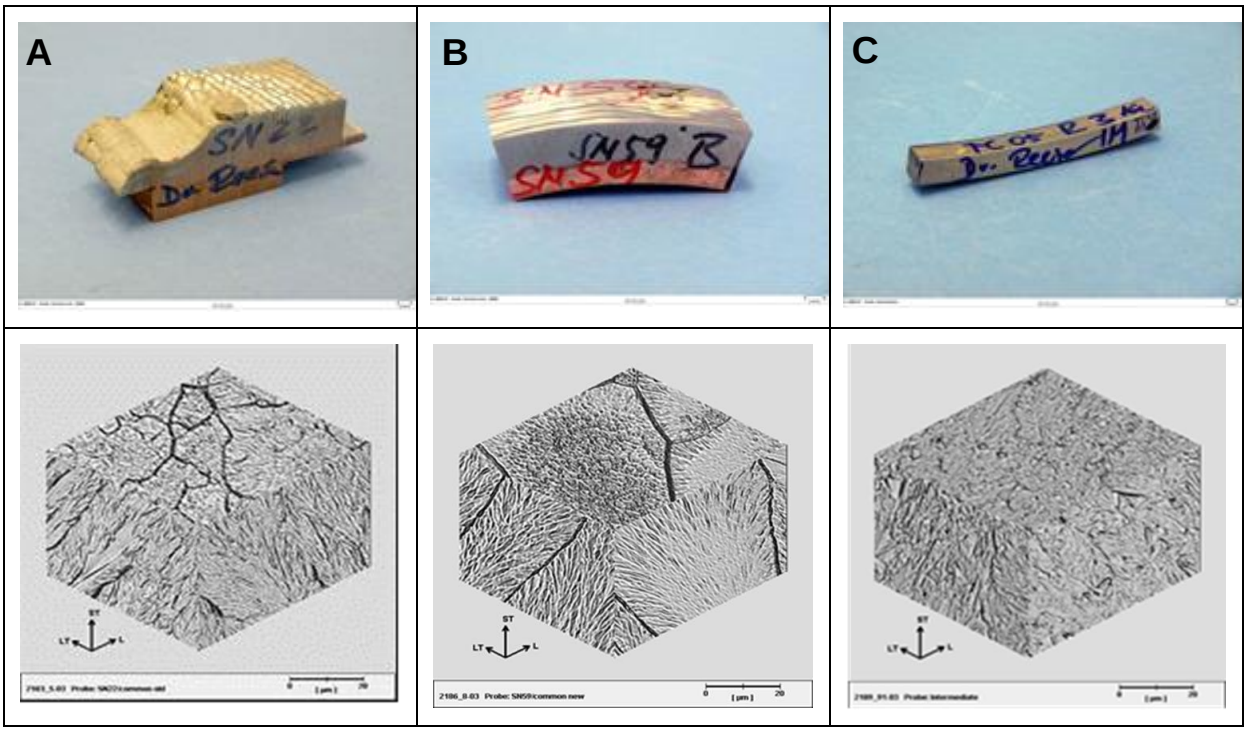

Figure 9: Samples of common old (A), common new (B) and intermediate (C) materials.

XRD measurements revealed a slightly preferred orientation of the (200) and (111) planes in the growth direction for all materials. TEM analysis detected presence of inclusions, likely originating from segregation of impurities. The TEM analysis also confirmed the existence of nanocrystalline regions in the “intermediate” materials.

Electron backscatter diffraction (EBSD) analysis was performed for all model materials. Due to the importance of grain boundaries on H diffusion in PP-Ni, EBSD analysis of the materials in CS1 focused on evaluating the grain boundary misorientation angles and the proportion of coincident site lattice (CSL) grain boundaries. High resolution scanning transmission microscopy (STEM) was also performed for the model materials in CS1. A key outcome of this analysis in CS1 was the detection of nanocrystalline regions in the intermediate PP-Ni material (see Figure 10). This highlighted the important role of grain boundaries in determining the rate of H diffusion in the PP-Ni materials.

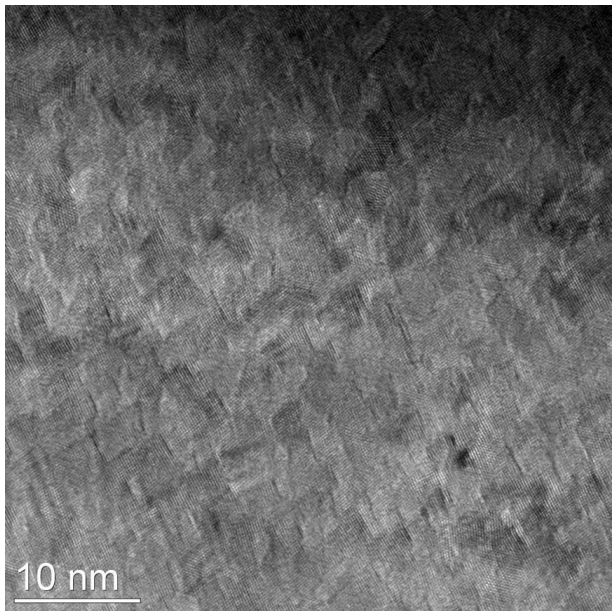

Figure 10: Nanocrystalline regions in the "intermediate" PP-Ni material.

CS2

A primary objective of CS2 was the evaluation of nano-sized Nb and Ti-carbides as a means of mitigating hydrogen embrittlement of advanced high strength steel (AHSS). Thus, a key part of microstructural analysis performed in CS2 focused on characterizing the distribution and morphology of Nb and Ti-carbides in the model materials using a variety of methods.

TKSE-concept steels

A key outcome of light microscopy analysis was that Ti has a grain-refining effect in all of the TKSE-concept steels. In the case of the tempered martensitic 1200TM09 and dual-phase 1200M04, the addition of Ti resulted in a reduction in the size of ferrite grains, although the fraction of ferrite in the steels with and without Ti was unchanged. The addition of Ti to the fully martensitic 1400M resulted in a reduction in the size of the martensite packets belonging to the same former austenite grain (Figure 11 and Figure 12).

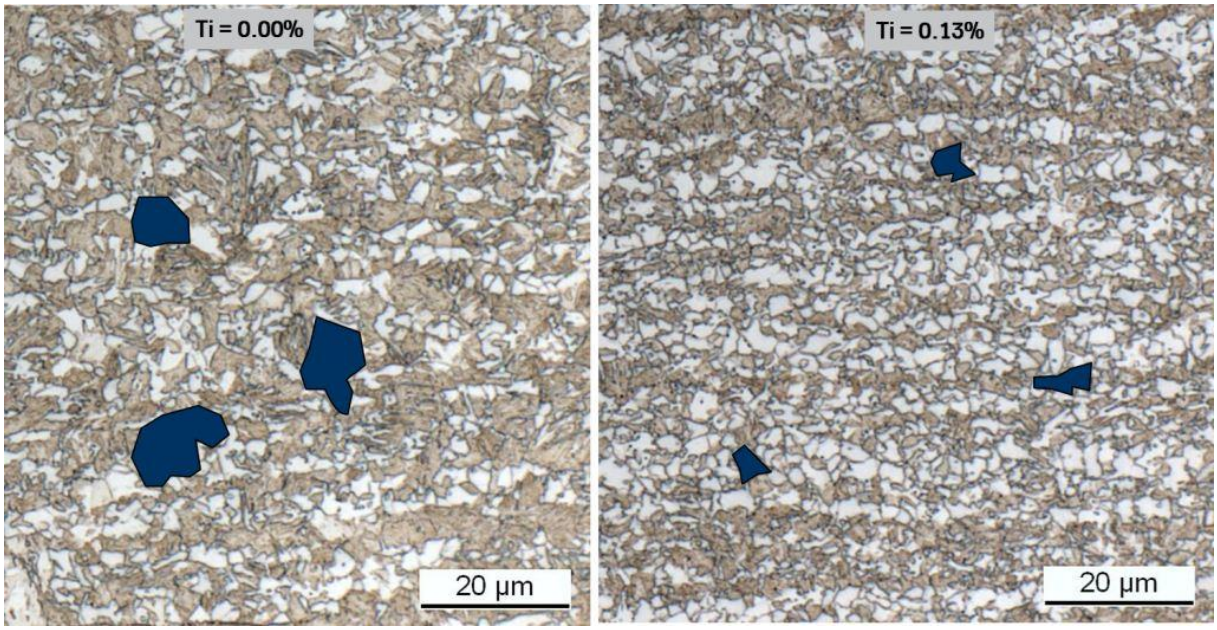

Figure 11: Effect of titanium on the austenite grain size for the grade 1200M04 (blue zones correspond to former austenite grains).

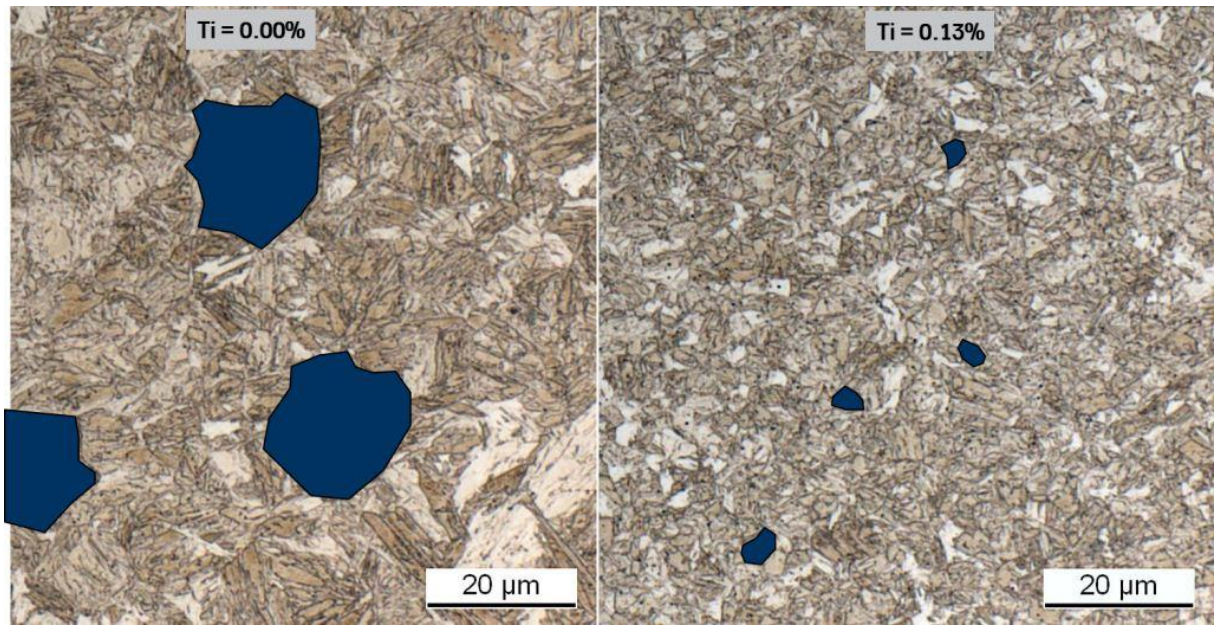

Figure 12: Microstructure and effect of titanium on the austenite grain size for the grade 1400M (blue zones correspond to former austenite grains).

Scanning electron microscopy (SEM) analysis was performed for all TKSE-concept steels in order to better evaluate the influence of Ti on their microstructures. In all materials, martensite takes the form of both lamellae and continuous packets. In the case of the dual-phase 1200M04 (Figure 13), ferrite is present between martensite as a coarse grain or sandwiched between lathes. The tempered martensitic grades 1200TM09 and 1400TM are characterized by Fe-carbides in the form of large flakes within the martensite (Figure 14). At these magnifications, the influence of Ti on the

size of ferrite grains is difficult to discern; however, its influence on the size of martensite grains is clear (Figure 14). Also apparent in some of the Ti-containing microstructures are small particles, which are presumed to be TiC, within both ferrite and martensite grains (Figure 13). The distribution of carbides in both phases is consistent with the proposal that the Ti-carbides are precipitated in the austenite matrix during annealing. A summary of the phase compositions of the TKSE-concept steels is given in Table 2.

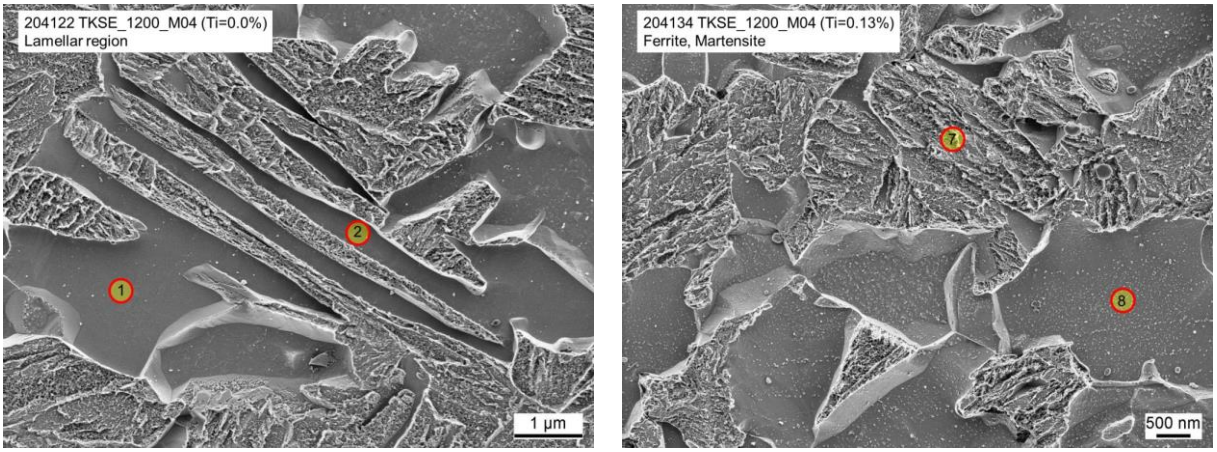

Figure 13: SEM-image for the grade 1200M04 with (A, right) and without (B, left) titanium.

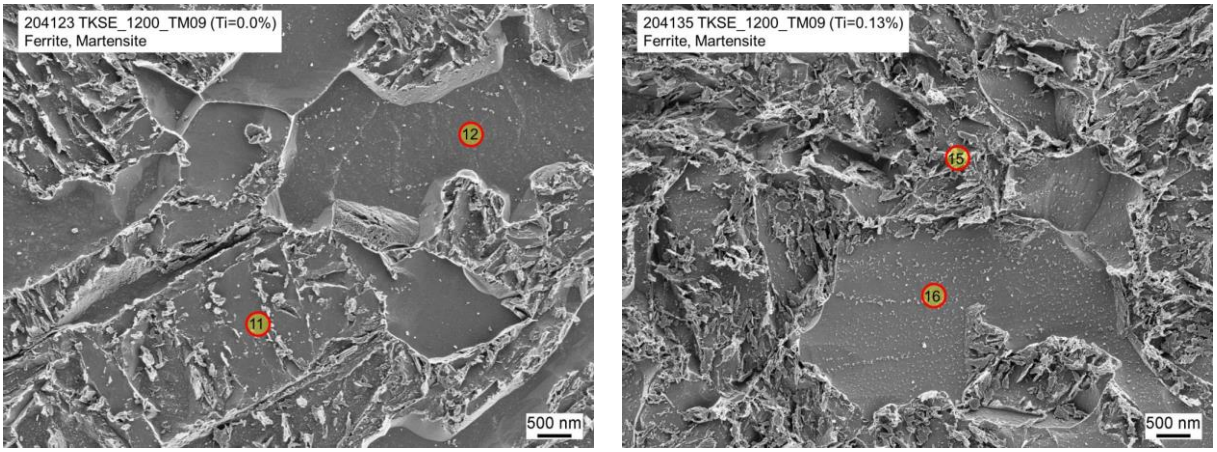

Figure 14: SEM-image for the grade 1200TM09 with (A, right) and without (B, left) titanium.

Table 2: Summary of the phase compositions of TKSE concept materials (no retained austenite was detected).

Material	Phase 1 (dominating)	Phase 2
Steels without Ti addition		
TKSE 1200 M04	ferrite (~60%)	martensite (~40%)
TKSE 1200 TM09	tempered martensite (~90%)	ferrite (~10%)
TKSE 1400 M	martensite (100%)	-
TKSE 1400 TM	tempered martensite (100%)	-
Steels with 0.13% Ti addition		

TKSE 1200 M04	ferrite (~60%)	martensite (~40%)
TKSE 1200 TM09	tempered martensite (~90%)	ferrite (~10%)
TKSE 1400 M	martensite (100%)	-
TKSE 1400 TM	tempered martensite (100%)	-

XRD analysis was performed for all of the TKSE-concept steels. It showed that retained austenite levels were below the 1% detection level in all microstructures and that the ferritic lattice constant remained at 0.2870 nm (+/- 0.0001 nm) for all microstructures (although peak broadening was not quantified).

Detailed analysis of the morphology and distribution of TiC particles in the TKSE-concept steels was performed using TEM and STEM (scanning transmission electron microscopy). TiC particles were detected in all four TKSE-concept grades. Due to the small sample size and high magnification of the TEM imaging it was impossible to perform statistical averaging of the particle characteristics; however, some general trends may be elucidated from the collected data. The particles were typically spherical or plate-like in appearance and ranged in size from 10nm to 250nm. They occurred in all phases, both within grains and at grain boundaries; no underlying tendency towards precipitation within certain phases or at certain microstructural features could be ascertained.

There is evidence in the literature[1] that H trapping by TiC particles is greatly affected by the nature of the particle-matrix interface, i.e. by the cohesion of the particle with the surrounding matrix and the level of misfit strain. High resolution imaging showed that the particles form mostly semi-coherent interfaces with the surrounding bulk phases (Figure 15). The image reveals that there are multiple defects in the matrix side of the particle-matrix interface, which likely correspond to misfit dislocations. Figure 16 shows STEM-EDXS images of the element distribution at a coarse TiC particle in 1200M04. There is an elevated concentration of Mn and Cr at the particle-matrix interface. Some Cr is also contained inside the particle.

[1] F.G. Wei, K. Tsuzaki, “Quantitative analysis on hydrogen trapping of TiC particles in steel”, Metallurgical and Materials Transactions 37A (2006) 331-353

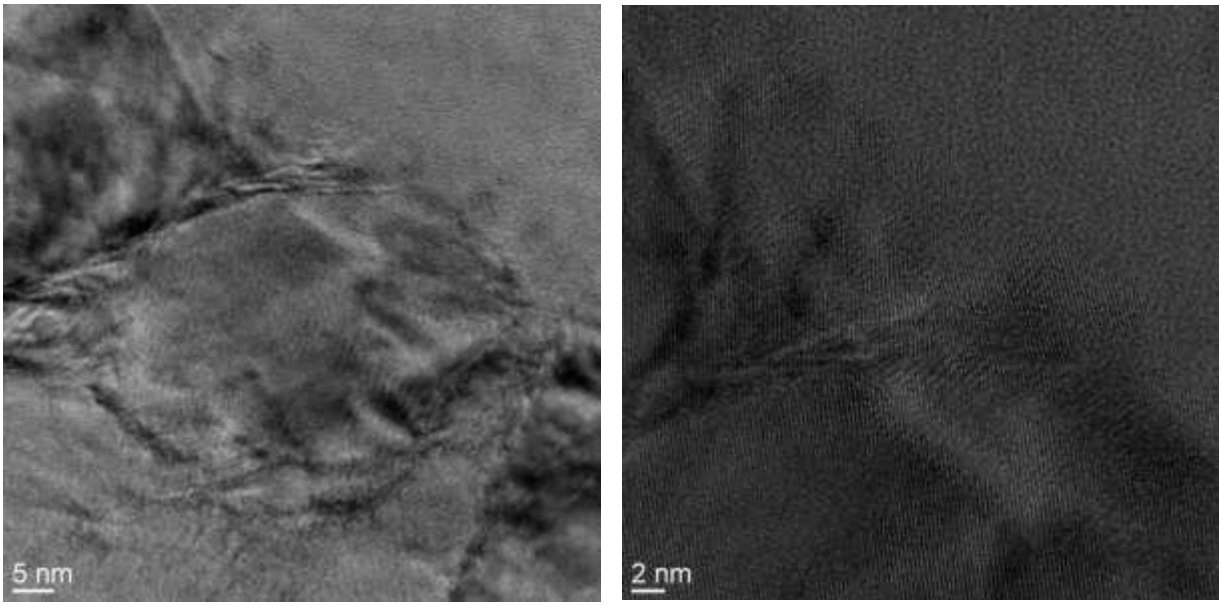

Figure 15: High resolution STEM images of TiC particle in 1200M04 showing defects at the particle-matrix interface.

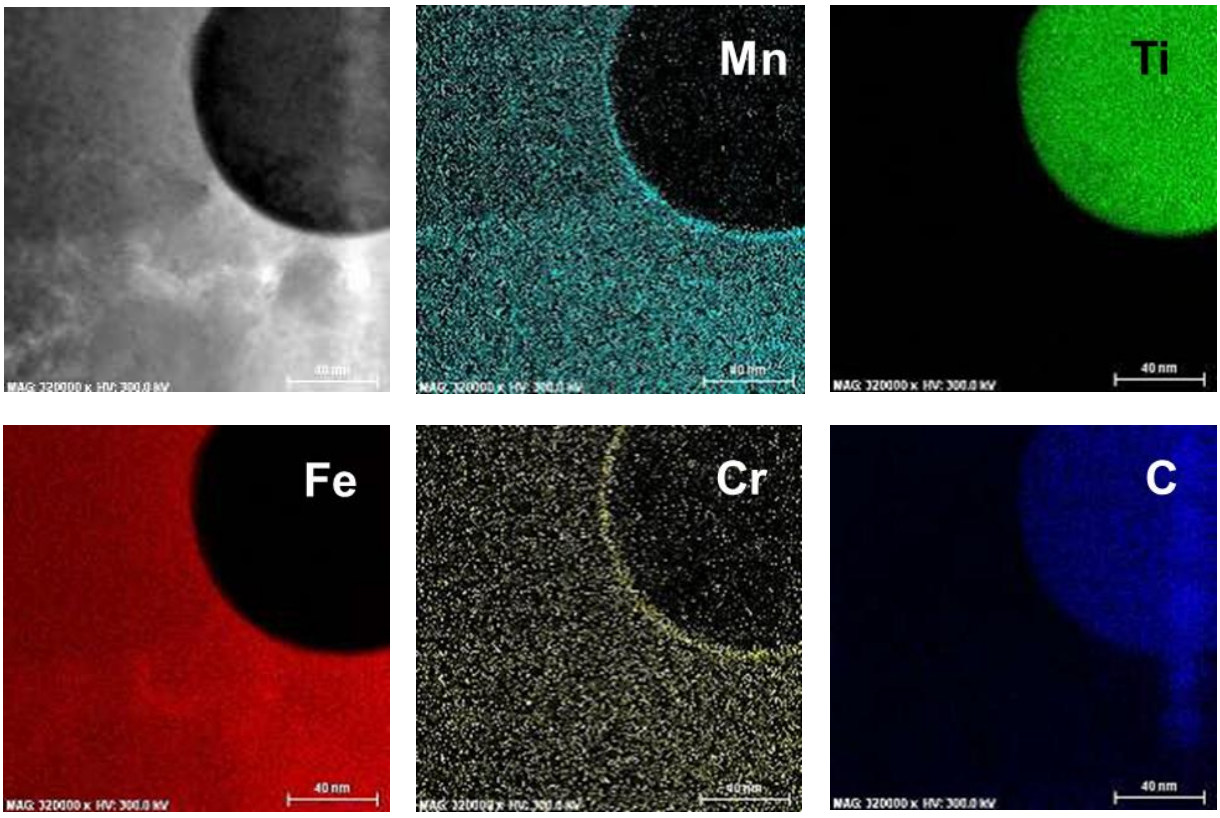

Figure 16: STEM-EDXS images of element distribution at TiC particle in 1200M04 with titanium.

VAS-concept steels

The light optical microscopy gives a first impression of the induced microstructures and explains their different mechanical properties like yield strength or elongation strongly related to their microstructure.

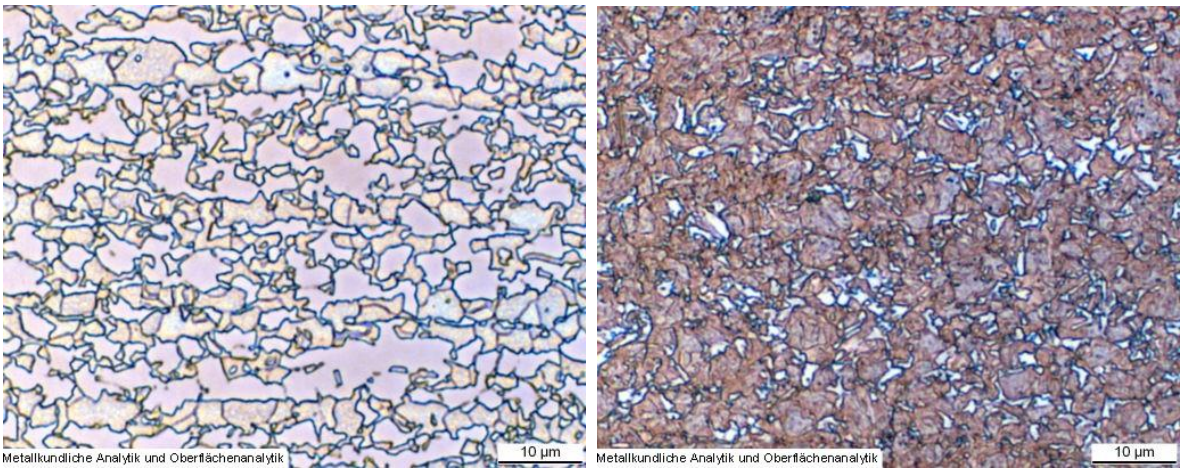

Figure 17: LOM images of 1200DP and 1200MTM containing 0,05wt.%Nb as an example for the different microstructures within strength class 1200MPa.

To quantify the different phases more detailed SEM investigations were performed for all microstructures. A summary of the phase compositions of the VAS concept steels is given in Table 3.

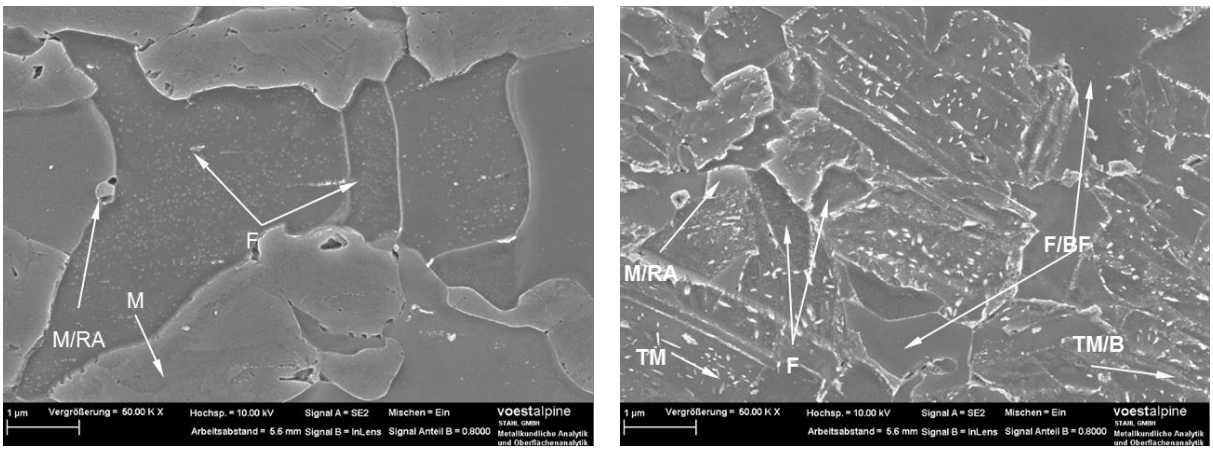

Figure 18: SEM micrographs of 1200DP and 1200MTM (0,05wt.%Nb)

Table 3: Summary of the phase compositions of VAS concept materials

Material	Phase 1 (dominating)	Phase 2	Phase 3	Phase 4
Steels without Nb addition				
VA 1200 DP	ferrite (~50%)	martensite (~50%)	retained austenite (≤1%)	-
VA 1200 MTM	tempered martensite/ bainite (~80%)	ferrite/ bainitic ferrite (~17%)	retained austenite (~3%)	-

VA 1400 TM	tempered martensite (~90%)	martensite (~10%)	retained austenite (≤1%)	-
VA 1400 MTM	martensite (~45%)	tempered martensite (~40%)	ferrite/ bainitic ferrite (~10%)	retained austenite (~4-5%)
Steels with 0.05% Nb addition				
VA 1200 DP	ferrite (~50%)	martensite (~50%)	retained austenite (≤1%)	
VA 1200 MTM	tempered martensite/ bainite (~70%)	ferrite/ bainitic ferrite (~25%)	retained austenite (~5%)	-
VA 1400 TM	tempered martensite (~90%)	martensite (~10%)	retained austenite (≤1%)	-
VA 1400 MTM	martensite (~50%)	tempered martensite (~25%)	ferrite/ bainitic ferrite (~20%)	retained austenite (~4-5%)

WP1.3: Numerical description of the microstructure

The main part of this work package was developing a numerical description of the microstructures that could be used directly in the numerical models. This proved to be most important in CS1, where it was anticipated that H diffusion in PP Ni would be affected by H interactions with grain boundaries. In light of the strong anisotropy of PP-Ni, modelling H diffusion necessitated the development of a numerical model of the grain boundaries. This has been done at the atomistic level by developing 3D models of Ni bi-crystals. At the macroscopic level, a procedure has been developed to process EBSD images of grain boundaries into a numerical form that can be used as an input to kMC and continuum models. This data, e.g. in a form of 2D array with elements corresponding to each pixel, were imported into continuum models to carry out simulations of inhomogeneous H diffusion.

WP1.4: Micromechanical testing

Micromechanical testing has been carried out to evaluate the hydrogen effect on the material mechanical properties in the nanometre range. These observations were related to the outcomes of the atomistic (WP4) and mesoscopic (WP5) modelling. The objective of WP1.4 has been to combine in-situ H charging with nanoindentation and micro-compression testing of FIB-cut pillars to evaluate the influence of H on mechanical properties of extremely small volumes of materials (see Figure 19).

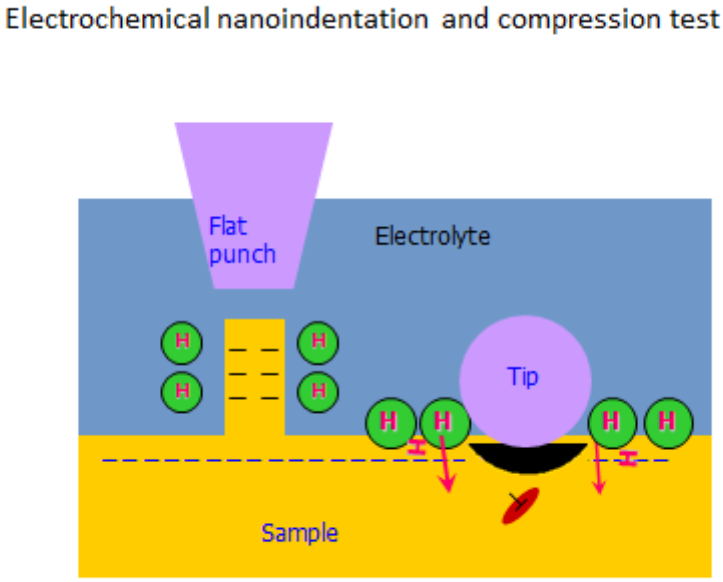

Figure 19: Schematic setup for electrochemical nanoindentation and compression testing.

The microstructural examinations (WP1.2) revealed presence of fine TiC-particles in the Ti-containing steel, while no carbides were observed in the Nb-containing steel. The micromechanical testing has therefore concentrated on the martensitic Ti-steels.

The micropillar compression tests showed that hydrogen reduces the flow stress, which is consistent with the HELP mechanism of hydrogen embrittlement. Under the same charging conditions, the amount of diffusible H in TiC-containing steel is less than in the Ti-free steel due to H trapping at the TiC particles. The reduction of the flow stress could be explained within the framework of the Defactant theory, considering the reduction in double kink nucleation energy in the presence of hydrogen [2]. This is in good agreement with previous experimental investigations on pure iron [3].

During the project, a novel potential-switch testing procedure has been developed in order to reduce the scatter of measured data due to sampling effects. This is

[2] R Kirchheim, “Solid solution softening and hardening by mobile solute atoms with special focus on hydrogen” (2012) Scripta Mater., 67 (9) pp. 767-770.

[3] H Matsui, H Kimura and S. Moriya, “The effect of hydrogen on the mechanical properties of high purity iron. I-softening and hardening of high-purity iron by hydrogen charging during tensile deformation”, (1979) Mater. Sci. Eng. 40 (2), pp.207-216.

achieved by switching the anode/cathode potential several times during the loading in order to examine the effect of H on the same pillar/microstructure.

While the pillars showed reduction in flow stress after hydrogen charging, the nanoindentation revealed an increase in hardness. The difference is not yet fully understood, but can be partly due to the complex surface structure of the martensitic microstructure and partly due to the difference in stress states affecting the trapping mechanisms.

3.2 WP2: Experimental determination of modelling parameters

3.2.1 Scope and objectives

The primary objectives of work package 2 were: (i) the determination of empirical parameters related to H diffusion and trapping as well as H-assisted fracture in the model materials; and (ii) the evaluation of the influence of microstructure and environmental and mechanical conditions on the susceptibility of the model materials to H-assisted degradation.

3.2.2 Summary of results

WP2.1: Electrochemical permeation testing

It was originally envisaged that electrochemical permeation tests would be performed “in-situ”, i.e. with simultaneous mechanical loading, using a cell previously developed at Fraunhofer IWM. However, a critical design flaw was discovered in this setup early in the project. A new cell capable of precisely measuring the H diffusion through the model materials (in the absence of external mechanical loading) was subsequently developed. The test procedure was validated by performing permeation tests on high purity Ni foils; the results of these tests were in good agreement with data in the literature. Permeation tests were then performed using samples of the model materials in all case studies.

CS1

H permeation through the PP-Ni materials in CS1 was generally faster than through pure Ni, with the permeation curves deviating significantly from the analytical solution to Fick’s second law. This suggested that the overall H flux was significantly affected by preferential H diffusion along grain boundaries and anisotropies of the PP-Ni microstructures.

In order to evaluate the influence of plastic deformation on the permeation behaviour of the PP-Ni materials, permeation tests were also performed for “common new” samples that had been pre-strained to 0.8% and 1.6% plastic strain. It was noted, that the overall rate of hydrogen diffusion through the samples decreased with increasing plastic strain. This effect may be attributed to the influence of hydrogen trapping by deformation-induced defects such as dislocations, vacancies, and microvoids.

Due to the nature of the pulse-plating process, it was anticipated that the permeation behaviour of the material would be dependent on the position from which the samples were machined from the combustion chamber wall. A comparison between the permeation curves for two uppermost samples - which were relatively consistent - and the permeation curve for an innermost sample showed a considerable difference. This suggests that the diffusivity of hydrogen in the material is macroscopically inhomogeneous.

CS2

In CS2, permeation tests were performed for the VAS and TKSE concept steels, with reference tests performed using the commercial steel CP1200. The addition of Nb to the VAS concept steels had negligible effect on H permeation. The influence of Ti on H diffusion in the TKSE concept steels was greatly dependent on microstructure, with the ferrite containing grades being most affected. A large number of tests were performed using CP1200 samples of thicknesses in order to validate the results (see Figure 20).

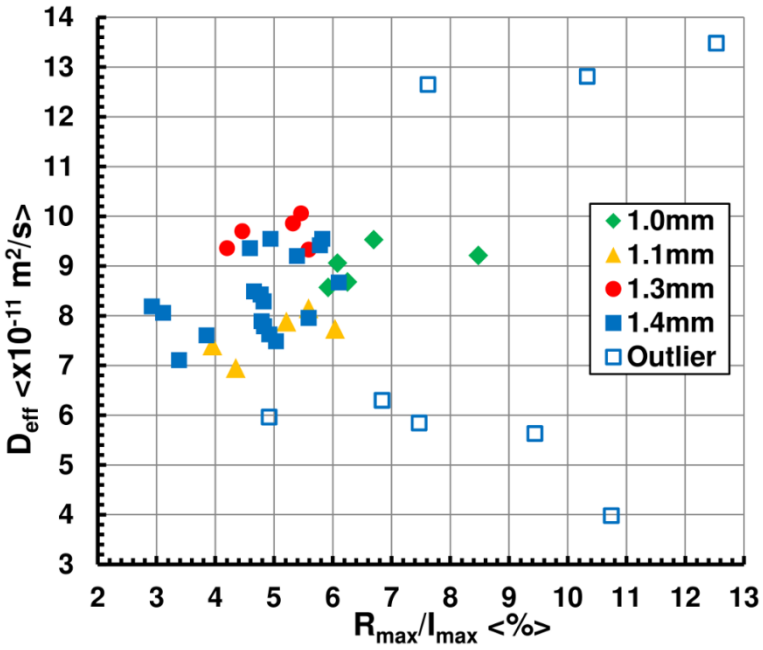

Figure 20: Effective diffusivity, Deff, vs the normalised residual with respect to the analytical solution to Fick's law, Rmax/Imax, for CP1200 samples of nominal thickness 1.0mm (■), 1.1mm (▲), 1.3mm (●) and 1.4mm (♦) as well as outliers (□).

CS3

Permeation tests were also performed by IWM using samples of the bearing steels in CS3; however, the results of these tests were generally unrepeatable. This may have been due to the relatively high sensitivity of the bearing steels to oxidation.

In order to obtain numerical values for McNabb-Foster equation, SKF developed a multi-parameter fitting procedure based on a genetic algorithm. The fitting procedure

provided the model parameters from the experiments to measure diffusion in bearing steels. One result of such a fitting is shown in Figure 21, where the result of an experiment with the Devanathan-cell is analysed using a six parameter McNabb-Foster equation. The graph shows that the model can be fitted accurately, thereby generating a realistic set of diffusion parameters.

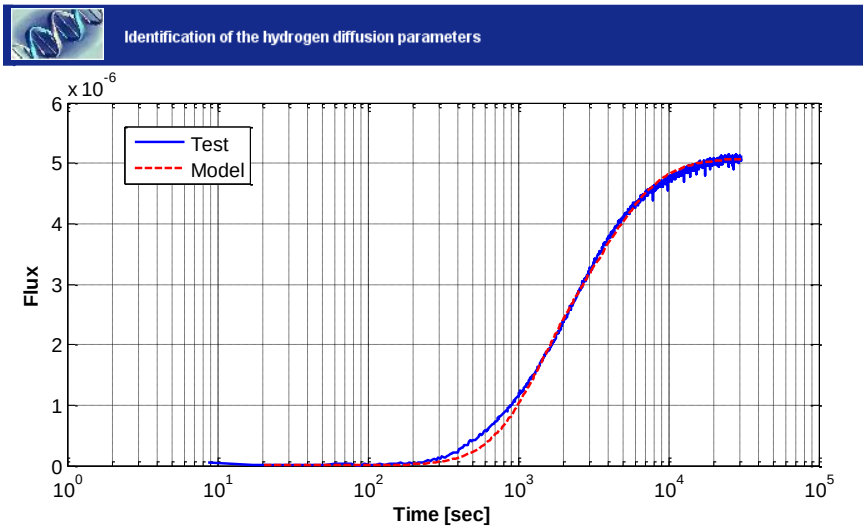

Figure 21 Experimental data of hydrogen diffusion in bearing steel and model.

WP2.2: Thermal desorption spectroscopy

CS1

Preliminary tests shown in Table 4 (last column) with non-charged CS1 material (see also WP3) revealed the approximate amounts of hydrogen introduced during production.

In order to prepare the samples for the determination of the activation energy, Airbus Defence and Space (formerly EADS) developed a charging procedure in a high pressure autoclave for the pulse plated nickel (PP-Ni) material. Four different variants (common-new, common-old, intermediate, pre-strained material) of the PP-Ni material were prepared using this procedure.

TDS measurements of the H-charged samples revealed an existence of two dominant traps. Traps with an activation energy of about 32 kJ/mol were detected in the desorption spectra of all variants (see Table 4) while a second peak with an activation energy of 93 kJ/mol appeared only in the spectra of the common new material (variant 1). This suggests that hydrogen trapping in the common new material is significantly stronger than in the common old and intermediate material. As a result, the differences in the total amount of desorbed hydrogen shown in Table 4 were attributed to the presence of the second peak in the desorption spectra. The pre-straining of the material (variant 4) did not affect the activation energy or the hydrogen content (see Table 4).

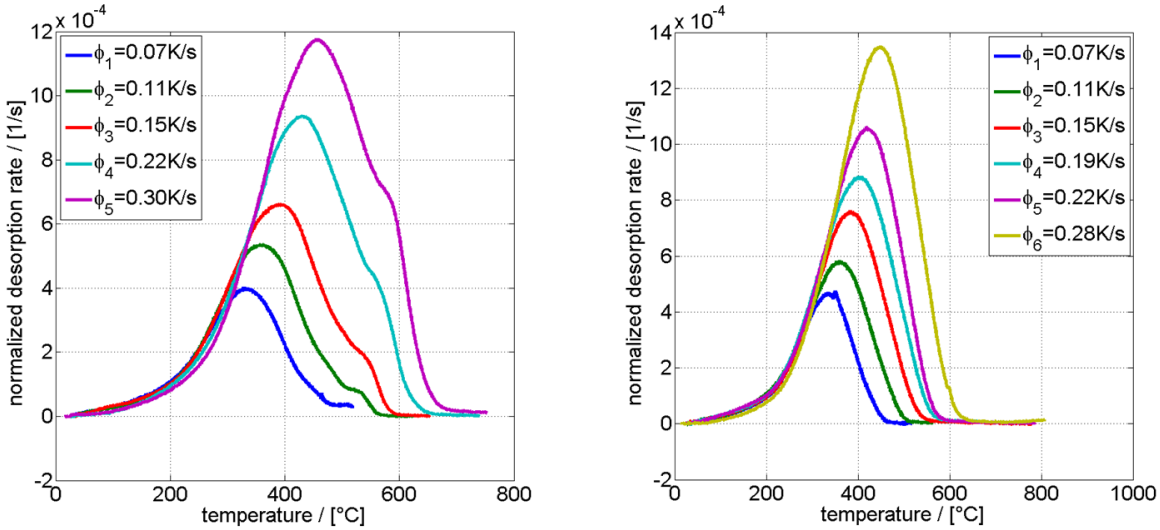

Figure 22: TDS spectra for the common-new (left) and the common-old (right) material.

Table 4: Summary of TDS results for the PP-Ni material.

	activation energy 1	activation energy 2	mean H-content	mean H-content (no pre-charging)
variant 1	30.1 kJ/mol	93.4 kJ/mol	21.96 ppm	3.46 ppm (2.87 ppm)
variant 2	32.9 kJ/mol	-	15.48 ppm	1.72 ppm
variant 3	31.74 kJ/mol	-	16.06 ppm	1.08 ppm
Pre-strained material	30.04 kJ/mol	-	15.52 ppm	-

CS2

A general problem in the thermal desorption measurements of ferritic steels is the fast hydrogen lattice effusion. Immediately after charging, the hydrogen at lattice sites and weak traps begins to effuse from the sample. As a result, even small changes in the transfer times to a liquid nitrogen storage after charging or during the sample preparation prior to measurement may lead to significant variations of the measured hydrogen content. Based on this observation, it was decided to introduce a step with controlled hydrogen effusion in the sample charging and preparation procedure in order to homogenise the hydrogen content of the samples, accepting the loss of hydrogen in flat traps and lattice sites.

A second issue was related to the testing equipment. Improvements were made to the TDS apparatus that reduced the measurement error by approximately 50%, thereby enabling the precise determination of activation energies. The inevitable

stepwise modification of the device caused some variations in the experimental results which, together with difficulties during sample preparation, lead to a loss of some specimens.

The test matrix for the thermal desorption analysis involved all the concept steels for CS2 with and without pre-straining. Figure 23 and Figure 24 show typical spectra and the corresponding plot used to determine the activation energy. Note that due to secondary effects the high temperature range had to be omitted from the analysis and traps with high activation energies could not be analysed with the available experimental setup.

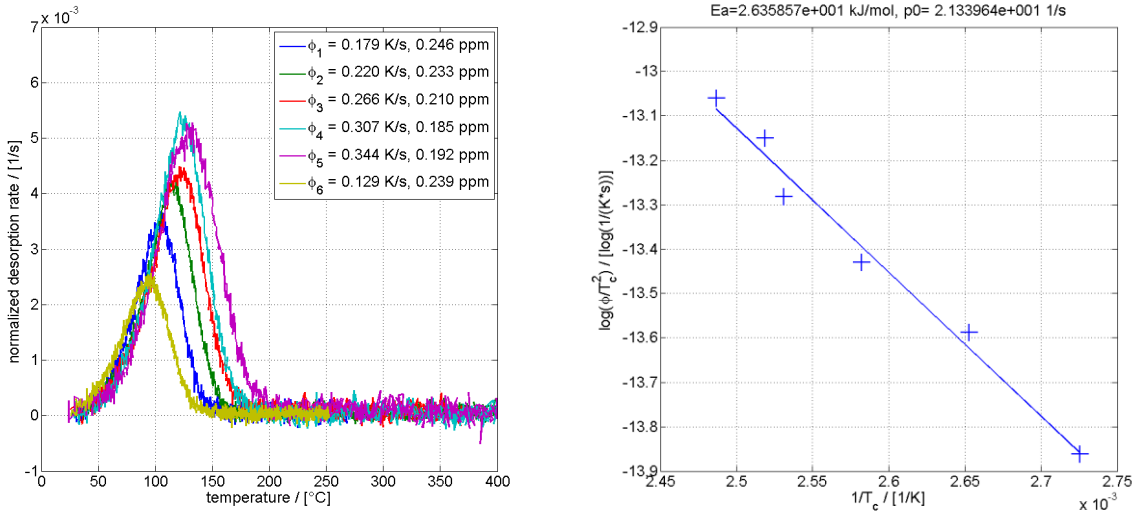

Figure 23: Normalized desorption spectra and activation energy plot for 1200M04 (0.00% Ti, 0.5% pre-straining).

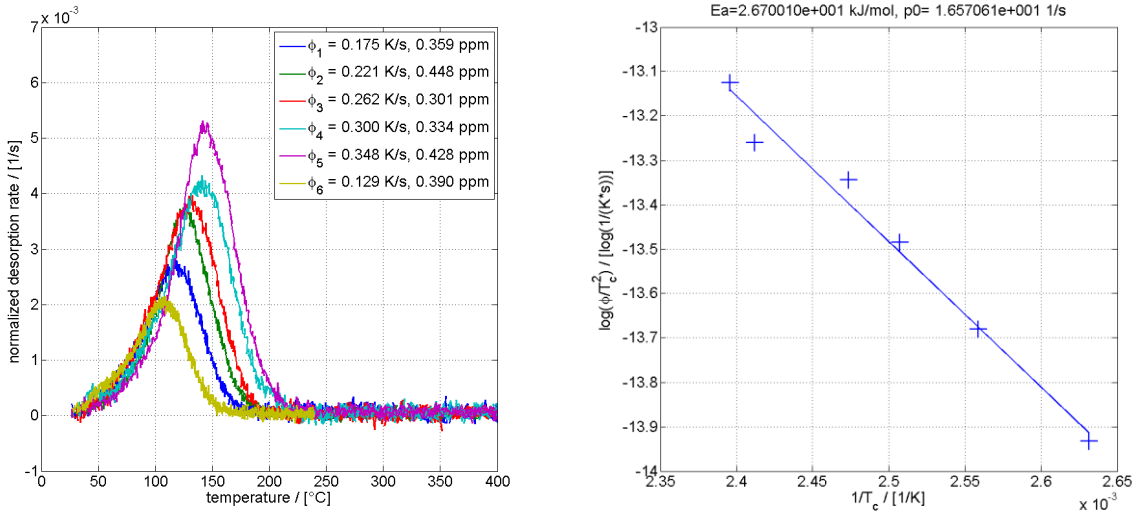

Figure 24: Normalized desorption spectra and activation energy plot for 1200M04 (0.13% Ti, 0.5% pre-straining).

The data obtained for all concept steels and pre-straining levels was subjected to a statistical analysis in order to verify general trends such as the postulated increase in hydrogen trapping for materials containing niobium or titanium carbides. The analysis revealed the following trends:

- pre-straining increases the hydrogen solubility
- the activation energy is independent of the pre-straining level
- the activation energy was almost independent of the microstructure (Figure 25)
- micro-alloying does not change the activation energy (Figure 26)

This analysis seemed to present evidence contrary to the assumption that titanium or niobium carbides act as particular trapping sites for hydrogen. However, based on these results, the trapping effect could not be strictly excluded owing to metallurgical (low trap density) and technical reasons (omitted high temperature range).

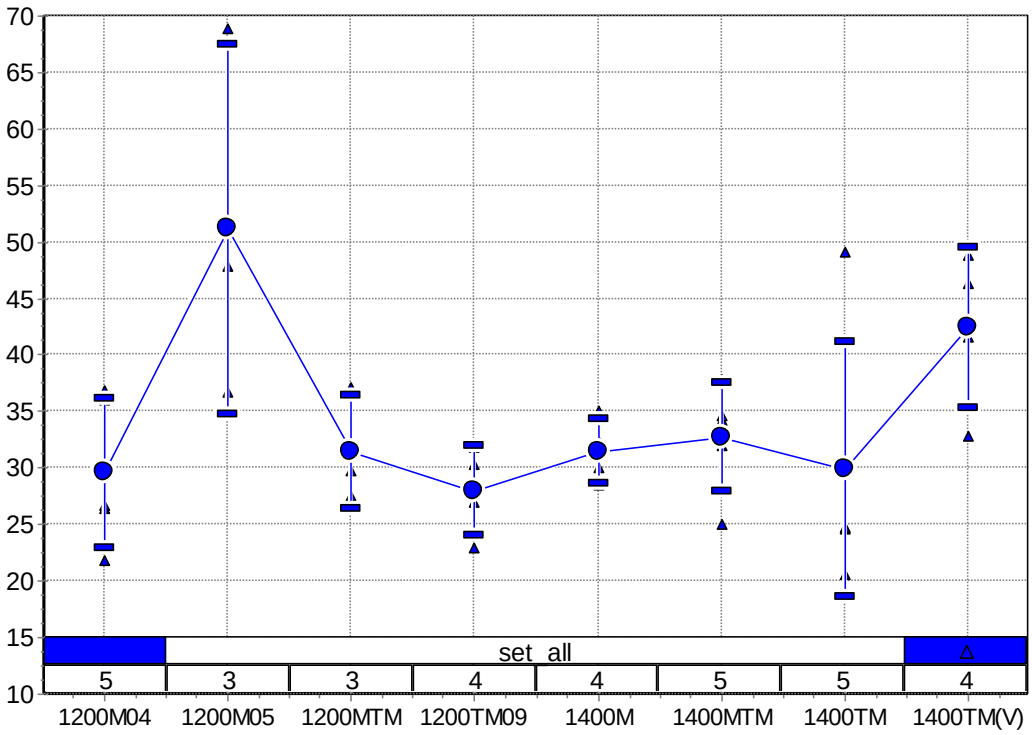

Figure 25: Activation energies obtained from TDS for different microstructures.

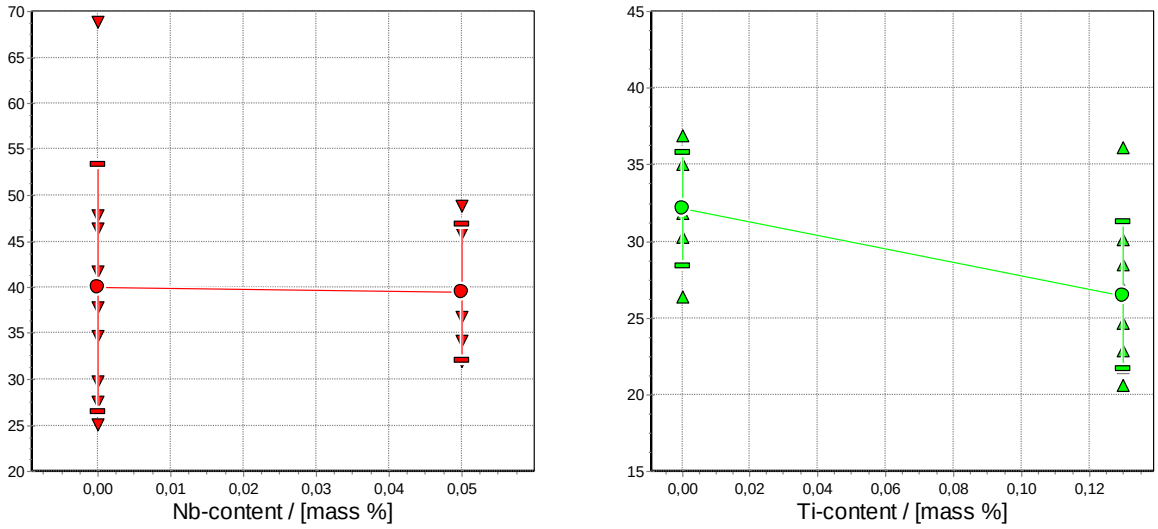

Figure 26: Micro alloying effect on activation energies (left: VAS-concepts with varying niobium-content, right: TKSE-concepts with varying titanium-content).

The results of the activation energy measurements did not show clear tendencies regarding the correlation between microstructure and hydrogen content. In a new series of measurements, a refined analysis of the hydrogen content was conducted for the TKSE concept steels (see Figure 27). In the absence of micro alloying elements, the hydrogen content was in the range 0.43±0.07 ppm for all microstructures. The micro alloying with titanium strongly affected the hydrogen solubility (equivalent to the hydrogen content) of the ferrite-containing concepts independent from the amount of ferrite (1200M04, 1200TM09), while the hydrogen solubility of martensitic concepts (1400TM, 1400M) was unchanged. This effect was attributed to the austenite grain refinement effect of titanium, which mainly affects the trap density of ferrite or ferrite-martensite interfaces.

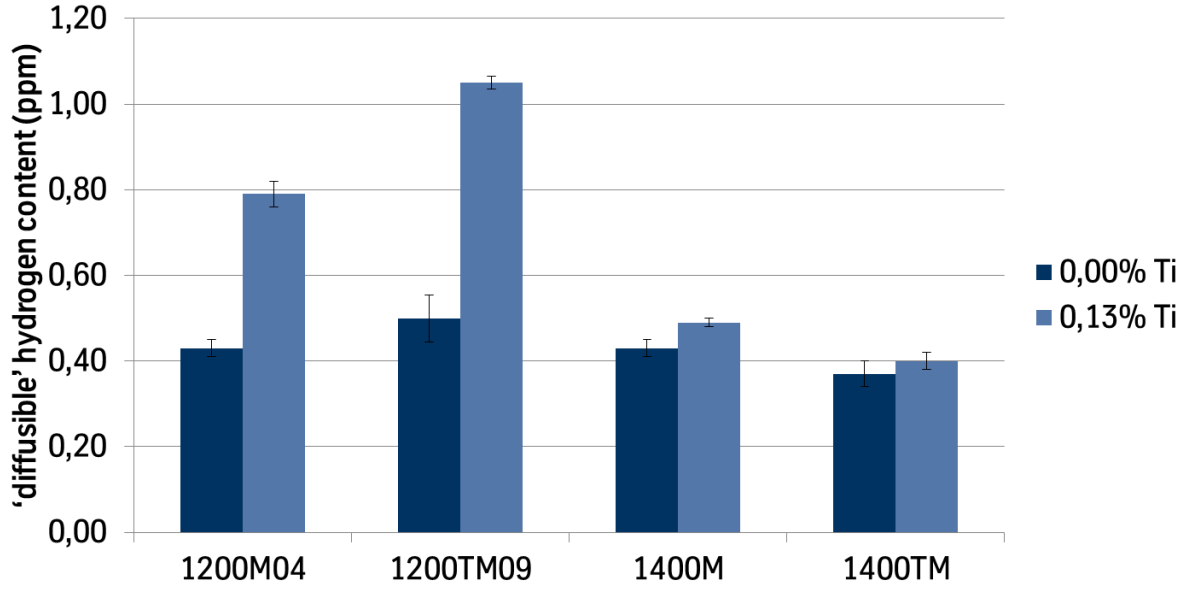

Figure 27: Hydrogen contents for the TKSE concepts with and without titanium.

WP2.3: Measurement of macroscopic thresholds

CS1

The susceptibility of PP-Ni to hydrogen-assisted degradation has been studied by investigating the influence of H-content on the fracture toughness. In addition to the hydrogen, which is incorporated during the production process ("naturally"), fracture mechanics coupons have been exposed to a gaseous H-atmosphere at elevated temperature and pressure in an autoclave.

Three levels of hydrogen concentration were tested:

- Condition A: samples with nominal H content in the as-coated condition
- Condition B: samples charged in H_2 atmosphere to saturation level
- Condition C: samples charged in H_2 atmosphere to saturation level and exposed to subsequent annealing

Measurements of H content revealed that the coupons reached a saturation value of about 30 ppm after already a few days. Overall, an even H-distribution was found in the samples. Electrochemical measurements showed an increased H-concentration in the vicinity of the notch. Standard fracture toughness tests showed that an increase in hydrogen content led to a significant decrease in fracture toughness. Out of the three PP-Ni-types, the intermediate material had the highest fracture toughness. When PP-Ni was welded onto an Inconel ring, a much lower H content in the HAZ than in the bulk material was detected.

CS2

In-situ constant extension rate tensile (CERT) tests were performed for all of the VAS and TKSE model steels as well as the commercial steel CP1200 (see Figure 28). In all materials, hydrogen charging resulted in a severe reduction in ductility and maximum tensile strength. It should be noted, however, that in most cases the H-charged samples failed with little or no plastic deformation. This suggests that the test results were affected by crack initiation at microdefects at the edges of the samples.

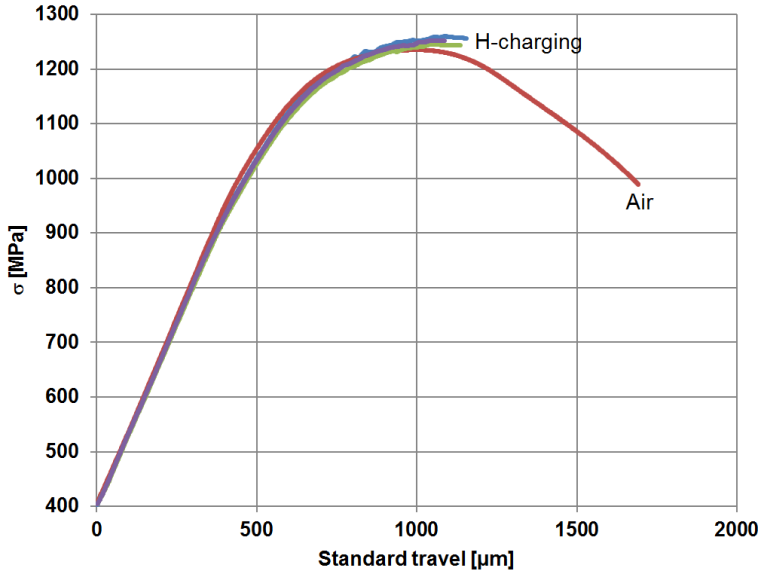

Figure 28: Stress vs displacement curves for CP1200 samples tested in air at 1.7x10-6 ms-1 and with in-situ cathodic charging at 1.7x10-9 ms-1.

CS3

The effect of hydrogen on Rolling Contact Fatigue was determined on basis of existing bearing tests. A number of tests were performed with hydrogen charged bearings and the results compared to those of standard uncharged bearings. The results show that the bearing life is reduced when the hydrogen content is increased. This phenomenon occurs at all contact pressure levels that were tested. This indicates that there may not be a threshold level at constant hydrogen level for the occurrence of hydrogen accelerated fatigue.

WP2.4: Fractography

CS1

A SEM investigation was carried out on fracture surfaces of hydrogen charged specimens of three variants of PP-Ni materials with different heat treatments. The fracture surfaces were prepared by static forced fractures under predominant mode I loading. The investigations of the forced fracture surfaces revealed that the presence

of hydrogen leads to brittle intercrystalline failure. The overall given hydrogen content is high enough, that intercrystalline crack growth can occur without time dependent hydrogen diffusion to the grain boundaries. With decreasing hydrogen content, increasing shares of ductile fracture morphologies can be observed on the forced fractures. The crack runs increasingly transcrystalline through the material. The still present hydrogen content has in case of the forced fracture no time to diffuse to the grain boundaries so that the still weakened grain boundaries can only be observed by secondary cracking. The local hydrogen content at the grain boundaries is not high enough to lead to intercrystalline failure. Time dependent fractures which allow stress induced diffusion of the hydrogen (e.g. creep rupture tests) were not carried out but would probably lead to intercrystalline failure also of the heat treated specimens with low hydrogen content. The comparison of not hydrogen charged fatigue areas with the static forced fracture after hydrogen loading reveal very similar fracture surfaces. This may be attributed to relatively weak grain boundaries of the base material even in the uncharged state. Comparing common old and intermediate material in the uncharged state shows pronounced ductile fracture with dimple formation. In contrast, hydrogen charged specimens after 3 h heat treatment show rather brittle, intercrystalline fracture appearance (Figure 29; Figure 30).

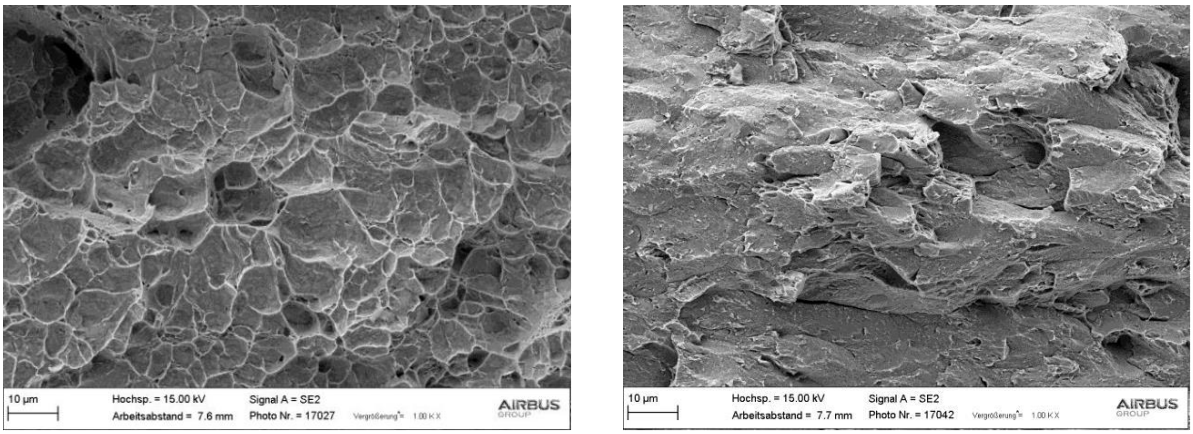

Not hydrogen charged

Hydrogen charged, 3h heat treatment

Figure 29: Common old – comparison of the fracture surfaces.

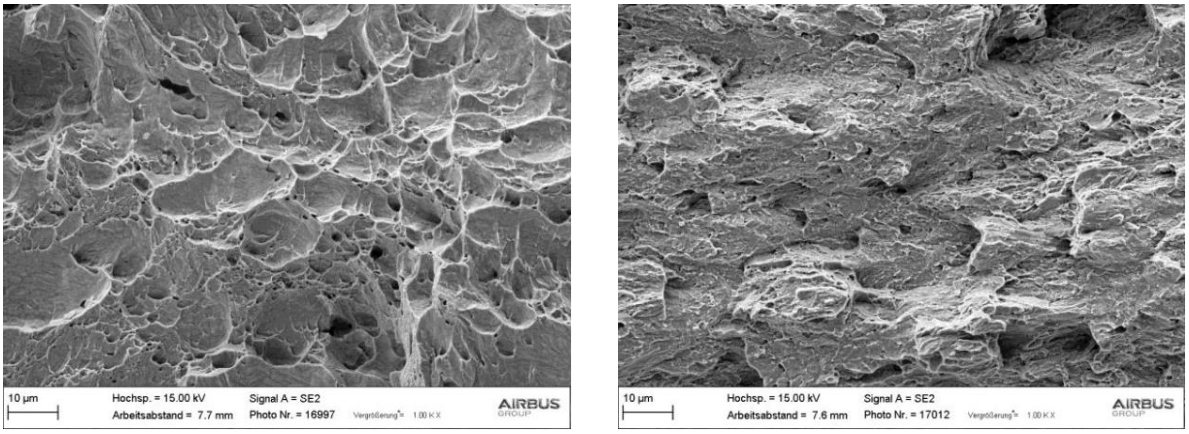

Not hydrogen charged

Hydrogen charged, 3h heat treatment

Figure 30: Intermediate – comparison of the fracture surfaces

CS2

Fractographic analysis of the AHSS samples tested in WP2.3 was carried out using scanning electron microscopy. Crack initiation in the H-charged CP1200 samples occurred at TiCN particles (seeFigure 31). For the model steels, crack initiation generally occurred at non-metallic inclusions or defects. Such inclusions may be the result of impurities present during the casting process and are not usually found in commercial steels. Thus, the susceptibility of the model materials to HE, as evaluated using the CERT tests, may not be representative of commercial steels.

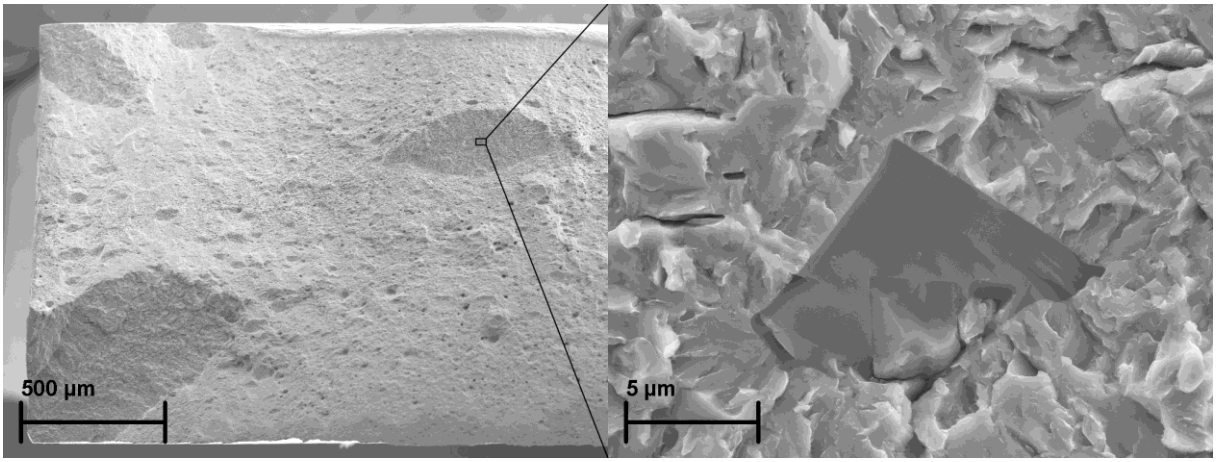

Figure 31: SEM image of the fracture surface of a CP1200 sample tested with in-situ cathodic charging at 1.7x10-9 ms-1 showing crack initiation at a TiCN particle.

CS3

To analyse the effect of hydrogen in the bearing inner rings, the rings were sectioned and etched for microstructure observation. Large crack networks were observed to develop in the sub-surface area of the bearings. The cracks were confined in the sub-

surface and did not cause a bearing failure. This means that hydrogen accelerates sub-surface fatigue processes. The fact that the damage occurs in the sub-surface zone confirms that subsurface fatigue starts at the location where the stresses are maximal.

3.3 WP3: Evaluation of process and service conditions

3.3.1 Scope and objectives

The objective of WP3 was to collect data from in-service observations and measurements that could provide the boundary conditions for the component models, as well as a "guiding range" for the atomistic/mesoscopic (WP4 – WP5) and continuum (WP6.1) models, and for the experimental determination of macroscopic thresholds (WP2.3). Data related to fractures occurring in service were also used for validation of the component models. The collected date included: (i) the position and mode of fractures occurring in service; (ii) information related to the condition of the component material (e.g. H-concentrations and residual stresses) after failure or after undergoing production processes suspected of causing failure; and (iii) the process parameters themselves.

3.3.2 Summary of results

WP3.1: Collection of process parameters and in-service data

Data collection for CS1

PP-Ni is produced via an electroplating process. The mechanical and thermal properties of PP-Ni coatings are greatly dependent on the characteristics of the current cycle and composition of the electrolyte. Electroplating inherently involves H evolution at, and absorption by, the cathode. The quantity of absorbed H is dependent on the cathode material, electrolyte and plating parameters (e.g. current density and frequency). For low current density, the H content is relatively low and independent of the frequency. But for lower frequencies, the H concentration increases with increasing current density. At high frequencies, the H concentration decreases slightly with increasing current density.

The amount of hydrogen absorbed in the structure is dependent on the effective current density, which may vary over the surface of the combustion chamber. Consequently, the H concentration is not uniform throughout the component. This dependency appears to be stronger for common-old and common-new type materials.

The H concentration of the PP-Ni may also be reduced by heat treatment at relatively low temperatures (in order to maintain the mechanical properties of the material) under vacuum.

After the plating process, two fuel manifolds made from Inconel 718 are welded onto the Ni-chamber. For reasons that are yet not well understood, longitudinal

cracks developed within hours or days (sometimes even longer periods) in the PP-Ni shell in the vicinity of the weld (Figure 32; Figure 33). It was observed, that the appearance of cracks seems to depend on the plating parameters and electrolyte used in the pulse-plating procedure.

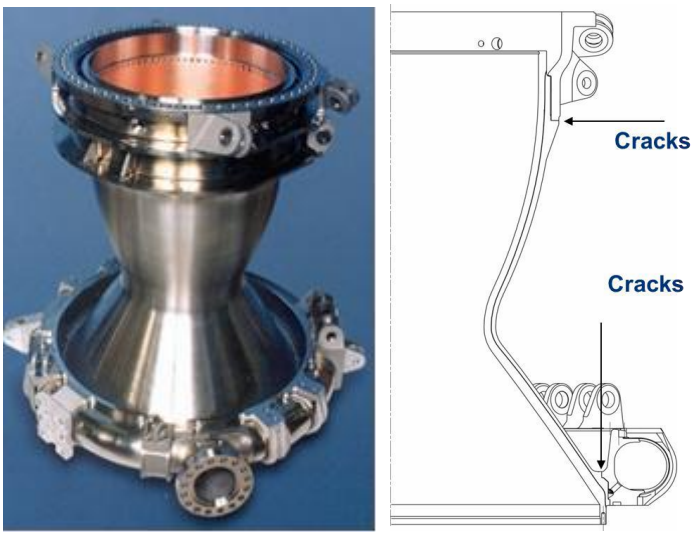

Figure 32: Location of cracks in PP-Ni-shell of the Vulcain 2 thrust chamber.

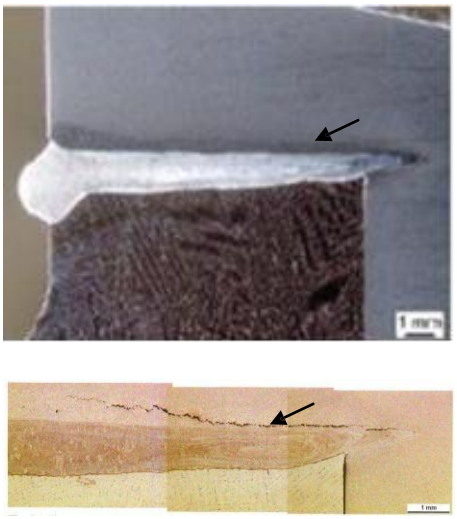

Figure 33: Cracks in PP-Ni-Shell.

It is assumed that H is the cause of this delayed cracking. The H concentration of the PP-Ni in the “as plated” condition seems to be uncritical. However, residual stresses resulting from the welding process are believed to cause H diffusion. This may eventually lead to the accumulation of H to critical concentrations and, consequently, H-embrittlement.

Residual stresses are present in the component as a result of heat introduced during the welding process. It is assumed that the H diffuses towards regions where tensile stresses are highest. Measurements have shown that residual stresses are highest in the vicinity of the weld seam and decrease rapidly with increasing distance from the weld seam. These tensile stresses, as well as cracks that have been attributed to H, are located outside of the weld-affected zone. Thus, cracking is not attributed to microstructural changes that occur as a result of heat input.

Based on the morphology and phenomenology of fracture, a failure hypothesis was proposed:

"The failure hypothesis assumes that small cracks are formed during the welding process. Due to the long-range welding-induced residual stresses, these cracks then act as a sharp notch around which tensile stress is concentrated. The tensile stress gradients act as a driving force for hydrogen diffusion, such that the hydrogen accumulates at the crack tip causing embrittlement of the surrounding material. This sequence occurs repeatedly, resulting in continuous crack growth over hours/days until the crack eventually reaches the surface."

Data collection for CS2

The main objective of CS2 was to quantitatively evaluate the conditions during the production of an automotive component made from Advanced High Strength Steels (AHSS) concerning the risk of HE. Two main processes during the production of a structural part of the body in white (BIW) were investigated:

- The coil production process in the steel plant.
- The painting process at the Original Equipment Manufacturer (OEM).

The strategy was to measure the hydrogen uptake during the most crucial steps within those processes for commercial AHSS grades as well as for alloying concepts containing trap forming elements Ti and Nb. In the next step the HE-resistance and hydrogen uptake behavior of those steel grades was distinguished. This data was used to simulate the HE-Risk of structural parts of the BIW for the highest possible hydrogen content introduced during the production process (refer to WP7).

AHSS grades used for assembling the body in white are generally delivered in the galvanized state. The electro-galvanizing is the most critical production step during which the material is charged with small amounts of hydrogen and sealed by the zinc coating. The trapped H can redistribute in the final part due to residual stresses introduced during forming step, and lead to HE if a local H concentration exceeds a critical value.

It was determined by VAS that the hydrogen uptake is strongly dependent on the operation mode of the galvanizing line with H concentration ranging between 0.1 and 1.0 wppm (total H content). Similar analyses were carried out by TKSE for commercial AHSS grades equivalent to those of the model materials used here.

From the subsequent processing by the automotive OEM, the most critical step for the overall hydrogen content is the painting process. This is includes a phosphatization process and cataphoretic painting during both of which H is produced on the steel surface and may diffuse into the bulk material. From measurements of H content performed at BMW, it was found that the hydrogen uptake during the BIW production is strongly depended on the microstructure of the steel grade but does not exceed in total 0.5 wppm (for commercial steel grades). The final H content was not affected by the final paint bake process.

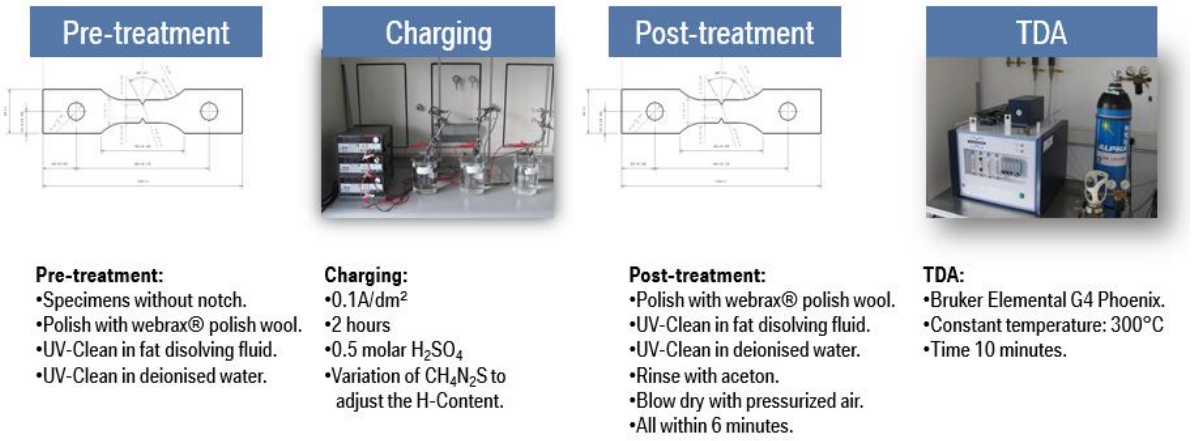

Figure 34: Illustration of the specimen production and the H-Content measurement in the Thermal Desorption Analysis (TDA).

To evaluate HE-resistance of AHSS in a reproducible and well defined manner, BMW probed a number of test specimens and testing conditions. A new reliable procedure (see Figure 34) for production of specimen used in notched tensile tests was developed and validated. These tests were used to obtain so called HE-embrittlement maps, shown in Figure 35 and Figure 36, which help to identify conditions for HE-risk in terms of the global H-content and the critical stress. The comparison of the HE-maps for two materials with comparable tensile strength but different microstructures (see Figure 36) shows a significant difference in HE-susceptibility. This data was thereafter used to postulate a fracture criteria (refer to WP7).

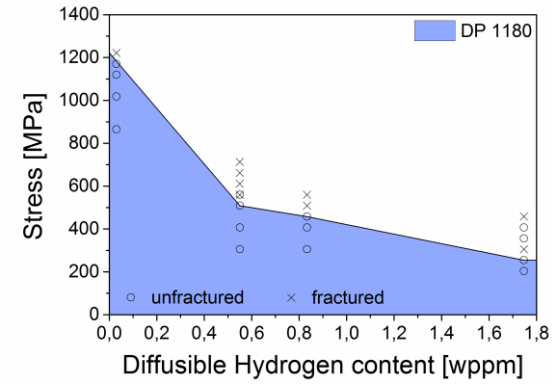

Figure 35: HE-map for DP1180

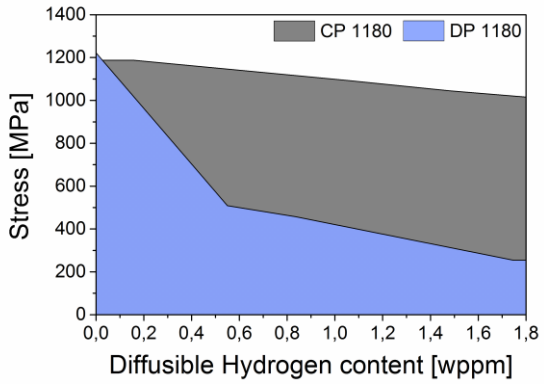

Figure 36: HE-map for DP1180 compared to CP1180

Finally, with this method it was possible to determine the HE-resistance and the hydrogen uptake behavior of all TKSE concept steels (see Figure 37, Figure 38 and Figure 39, Figure 40 respectively).

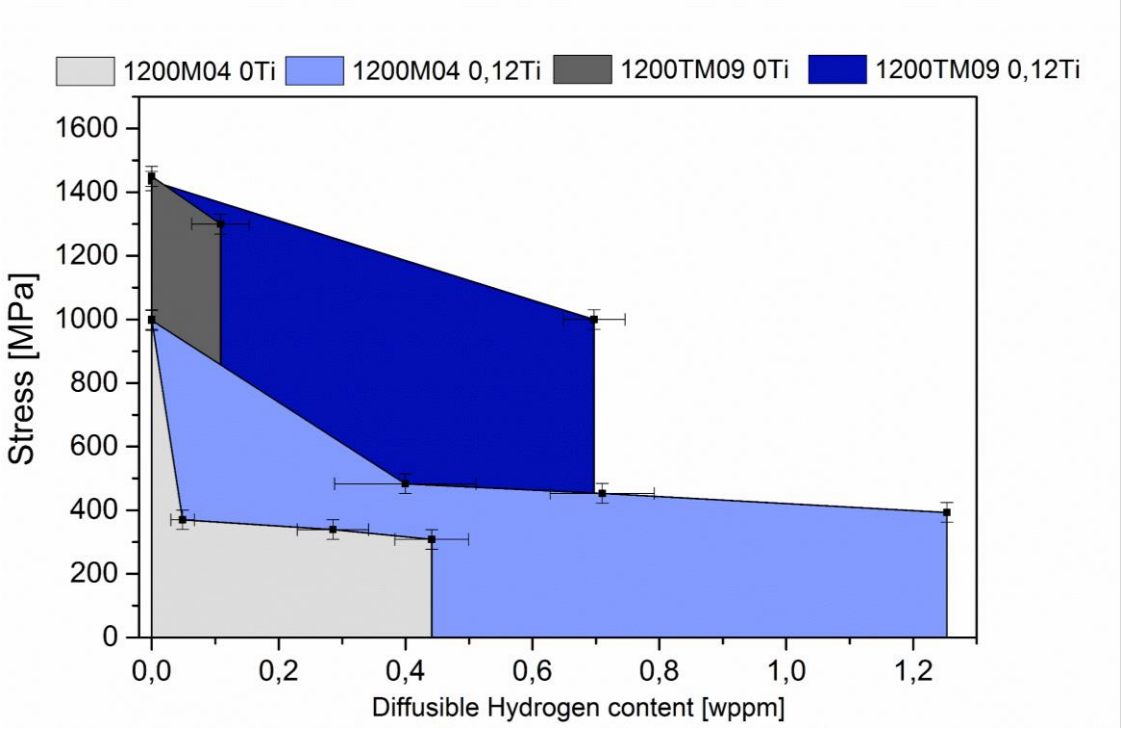

Figure 37: HE-map for all alloying concepts with a tensile strength of 1200MPa.

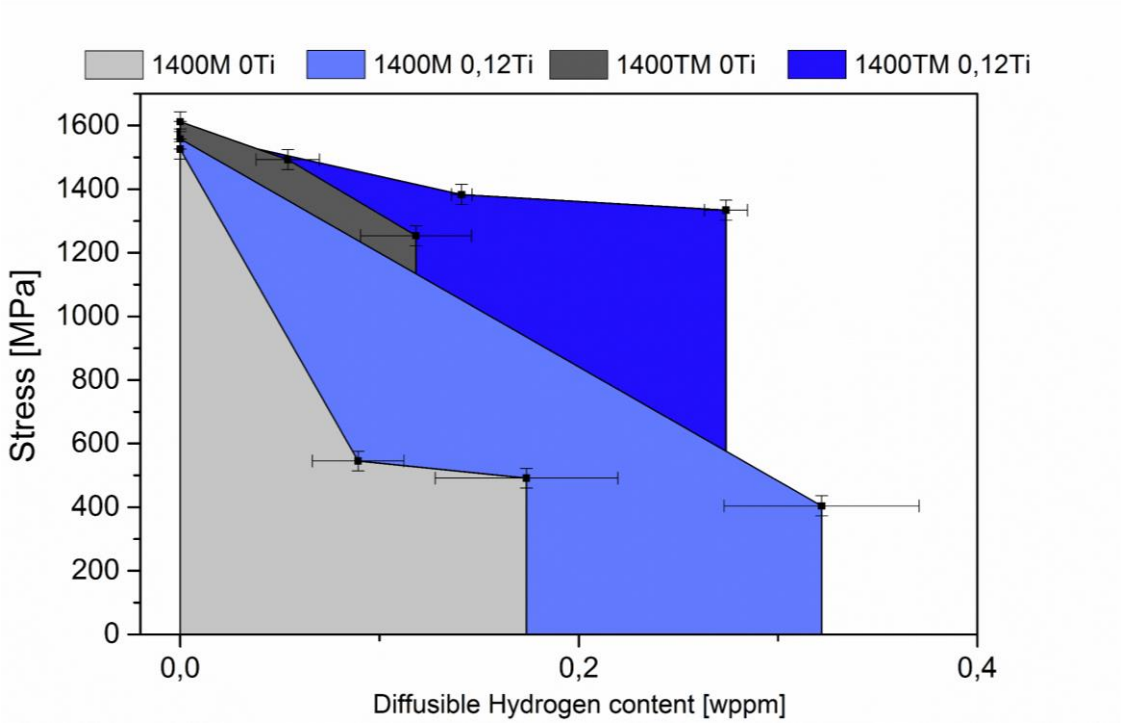

Figure 38: HE-map for all alloying concepts with a tensile strength of 1400MPa.

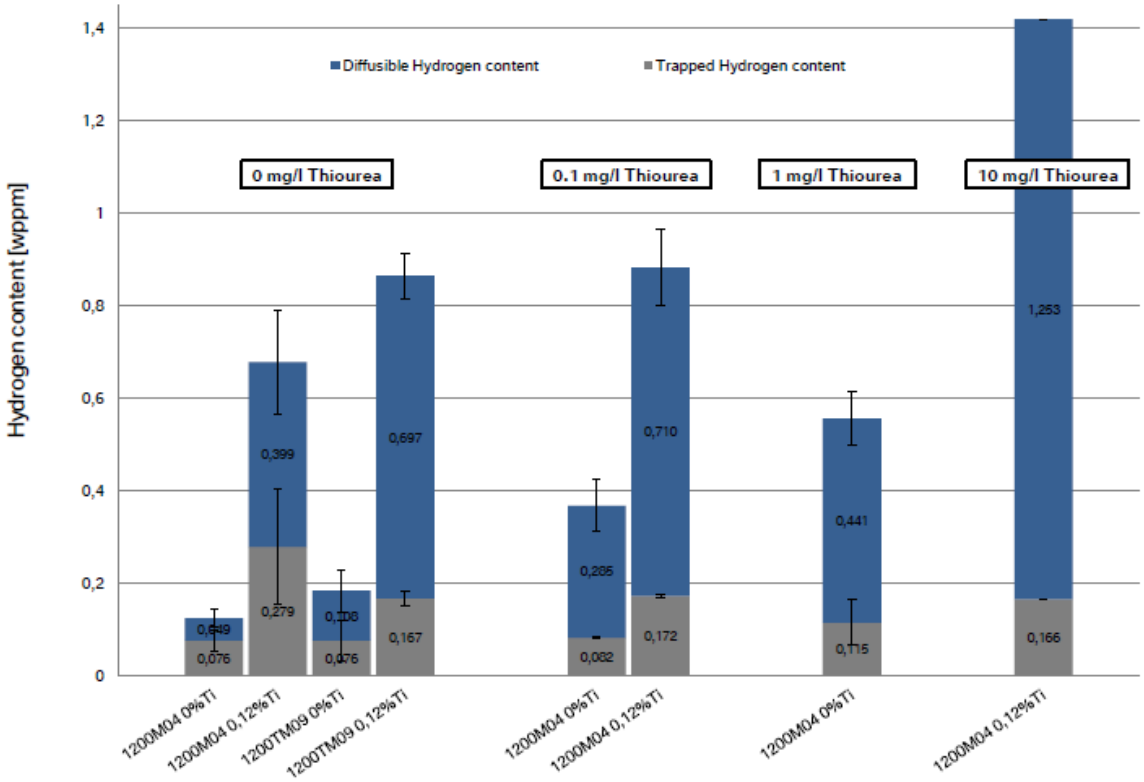

Figure 39: Hydrogen uptake behavior for all alloying concepts with a tensile strength of 1200MPa.

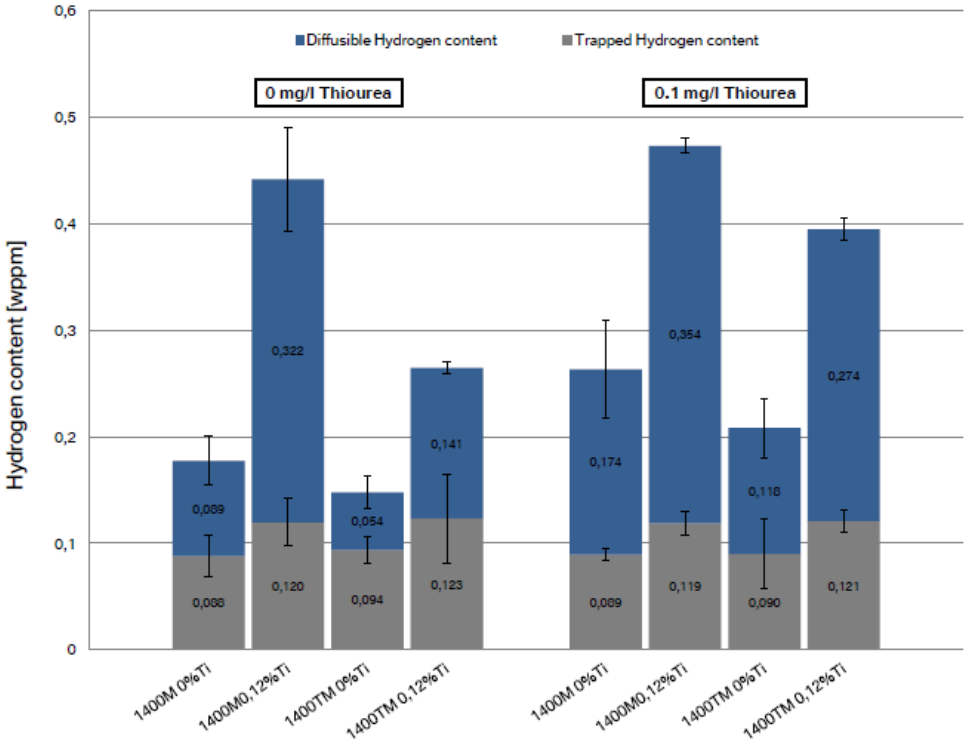

Figure 40: Hydrogen uptake behavior for all alloying concepts with a tensile strength of 1400MPa.

Two major conclusions drawn from these results are that (i) Ti alloying increases the HE-resistance for specimens with the same H-content, and (ii) the addition of Ti increases the hydrogen uptake behavior if charged under the same conditions.

Due to the promising results of the MultiHy project the notched tensile test was accepted as a first HE-test in the BMW homologating process of AHSS grades with a tensile strength above 1000 MPa. At the moment this HE-test is being evaluated in the VDA (Verein Deutscher Automobilhersteller) for HE in order to become a standardized HE-test.

Data collection for CS3

The objective of CS3 was to provide details regarding operating conditions for wind turbine bearings leading to premature failure due to H-assisted rolling contact fatigue. A detailed review of incidents was performed in which HA-RCF was suspected to be the cause of failure. This resulted in the development of a hypothesis for the role of H in bearing failures. Collection of quantitative data from wind turbines in service has proved to be more difficult due to such data being owned by the wind turbine operator. However, some microstructure investigations were carried out. In addition, simulations were performed using SKF's "BEAST" simulation tool, which enables the determination of the loading conditions in the bearing corresponding to the full-scale bearing tests and extreme operating conditions, as well as a small size Tapered Roller Bearing (TRB) that can be used for validation of hydrogen transport and diffusion models in future.

Early failures of main gearbox bearings in wind turbines under normal operating conditions are often attributed to absorption of H by the bearing material from the environment. The actual source of H is not fully understood. Possible sources of H include: (i) localised corrosion during standstill due to acidic components in the lubricant; (ii) catalytic decomposition of the lubricant due to non-lubricated contact; and (iii) electrolytic effects induced by stray currents or electrical voltage differences. Absorbed H may diffuse several millimetres into the sample over weeks or months during operation. Once in the steel matrix, H atoms interact with the crystal defects and accelerate fatigue damage, especially at non-metallic inclusions. Subsequent crack propagation is also enhanced by H such that cracks may become very long. Rubbing between opposite crack surfaces may result in recrystallization, which is manifested by the so-called white etching area (WEA) (Figure 41). Propagation of the WEA- decorated cracks eventually leads to spalling, i.e. pieces of material falling out from the raceway. The onset of spalling is considered to constitute the end of the bearing life, as failure of the bearing ensues very quickly thereafter.

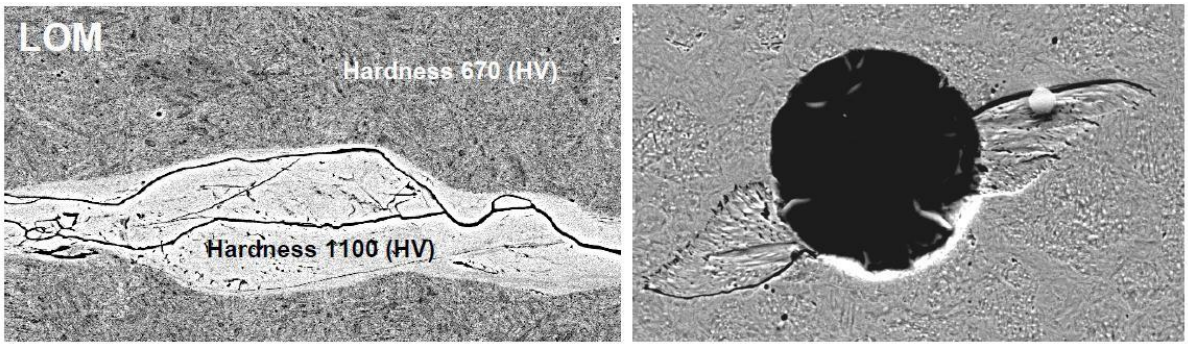

Figure 41: Examples on white-etching areas (WEA) induced by rolling contact fatigue of wind-turbine bearings.

Simulations using SKF's BEAST simulation tool were performed in order to determine the dynamic condition (e.g. transient contact pressures) insider the bearing under conditions representative of those occurring in service and in full-scale bearing tests.

3.4 WP4: Atomistic modelling

3.4.1 Scope and objectives

H mobility in metals is strongly affected by lattice defects such as vacancies, dislocations, grain boundaries (GBs), and phase interfaces. Vacancies, dislocations and phase interfaces act as trap sites for diffusing H atoms and hence lower the effective H diffusivity. Grain boundaries are typically assumed to be fast diffusion pathways for H due to their more open atomic structures.

The main goal of the atomistic simulations within WP4 was to investigate the binding energies and diffusion barriers for microstructural features and defects relevant for the project case studies. In CS1 (pulse plated nickel layers with complex microstructures composed of sub-micron grains), grain boundaries are likely to play a critical role in H transport. In CS2 and CS3 (steels for ball bearing and automobile applications), a broad range of microstructural features and defects may affect H transport; however, the main points of interest are nano-sized carbide precipitates (e.g. Ti and Nb based carbides), point defects and defect clusters.

3.4.2 Summary of results

WP4.1: Influence of strain on hydrogen diffusion in bulk phases

Atomistic simulations using first principles calculations based on the density functional theory (DFT) were carried out to investigate the energetics of high-symmetry H interstitial sites (octahedral, tetrahedral, saddle points) in bulk phases of body-centred cubic (bcc) Fe and face-centred cubic (fcc) Ni. In order to provide input for the kinetic Monte Carlo simulations we also studied the energy barrier associated with the jump of H between neighbouring interstitial sites. These calculations were

carried out using the so-called nudged-elastic band method, which is nowadays a standard method for finding the minimum energy pathway (MEP) between two states of a system. The MEPs were investigated in both metals as functions of H concentration and lattice deformation. The general trend in all cases is that the barrier height decreases with decreasing H concentration and increasing expansion of the lattice. Apart from the influence of hydrostatic strain, the changes of migration barrier under other deformation modes, such as uniaxial tension and compression, and pure shear strain, were also examined.

The computed migration barriers are markedly larger in fcc Ni than in bcc Fe system. This result is consistent with experimental observations that find H diffusivity to be generally faster in metals with bcc lattices.

Since H is the lightest element, its diffusion through the crystal lattice cannot be described at all temperatures as thermally activated over-barrier jumps (i.e. by a classical transition state theory), but quantum-mechanical effects such as tunnelling need to be considered. In order to account for these effects, we computed the quantum corrections using several theoretical approaches (Flynn & Steneham model, semiclassically corrected harmonic transition state theory, Feynman path integral method). According to all these theories, it is crucial to include the quantum corrections when describing H diffusion in the bcc Fe-H system where the barrier height is very small. Even at ambient temperatures, the quantum corrections cause a reduction of the classical barrier by about 50%. The theoretically predicted temperature dependence of the diffusion coefficient agrees very well with the most recent experimental data. Similar calculations were done also for the Ni-H system. Since the barrier height exceeds several tens of eV, the quantum corrections are less important in this system.

WP4.2: Case-study specific atomistic calculations

Atomistic modelling in CS1

We explored H interactions with several types of GBs in Ni in order to explore behavior of H in distorted atomic environments. Both the segregation of H at various interstitial sites in the vicinity of the GBs and the migration of H towards and along the GBs have been studied in detail. Our calculations revealed that different GBs can have a markedly different interaction behavior with atomic hydrogen and that the H trapping and migration depend strongly on the GB character. Special GBs with coherent atomic structures, e.g. deformation twins, neither trap H nor enhance its diffusion, but instead act as a two-dimensional diffusion barrier. In contrast, general GBs with more open atomic structures provide numerous trapping sites for H within the open structural units as well as easy migration pathways for H diffusion along the GB plane that can enhance the H diffusivity up to two orders of magnitude compared to bulk Ni. The obtained results are consistent with those of other computational and experimental studies. Based on comparisons with available literature data, we presume that the investigated GBs can be considered as representatives for a larger variety of GB types. The results obtained for Ni can be also transferred to other

metals, but it is always necessary to consider the GB effects with respect to bulk diffusion. If the bulk diffusion is sufficiently fast, the effect of enhanced diffusion along GBs can be negligible, or the trapping may even prevail.

In addition to the diffusion properties, we also studied the H solubility at GBs, and whether and how significantly H affects the GB cohesive strength. We found that the amount of segregated H at the general GBs can be relatively large and that the presence of H strongly influences the structural and mechanical properties of these GBs. Both static and dynamic simulations confirmed that H segregation contributes significantly to weakening of GBs and promotes intergranular fracture.

Atomistic modelling in CS2

Experimental observations have suggested that nano-sized transition-metal-carbide precipitates (e.g. TiC, NbC, or VC) can act as efficient trapping sites for H, but a quantitative description of the underlying atomic scale mechanisms has been lacking. In order to identify the possible trap sites and to quantify their strength and effectiveness, we investigated the interaction of H with TiC particles in bcc iron matrix at the atomic scale using first principle calculations. Various trapping sites at coherent, semi-coherent, and defective TiC/matrix interfaces as well as trapping at carbon vacancies within the TiC precipitates were investigated. The most significant results of our calculations are summarized in Figure 42.

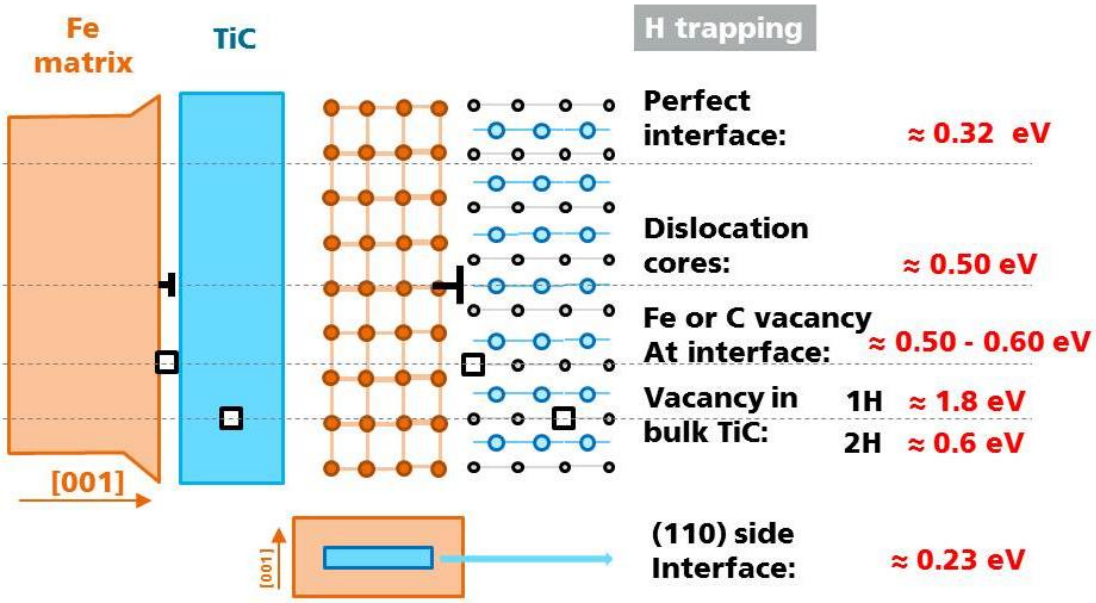

Figure 42: **Summary of trapping energies at various TiC obtained.**

In order to test the validity of these theoretical predictions, we carried out a detailed comparison with available experimental data. As shown in Figure 43, our calculated

values agree very well with the experimentally derived trapping (also known as desorption) energies.

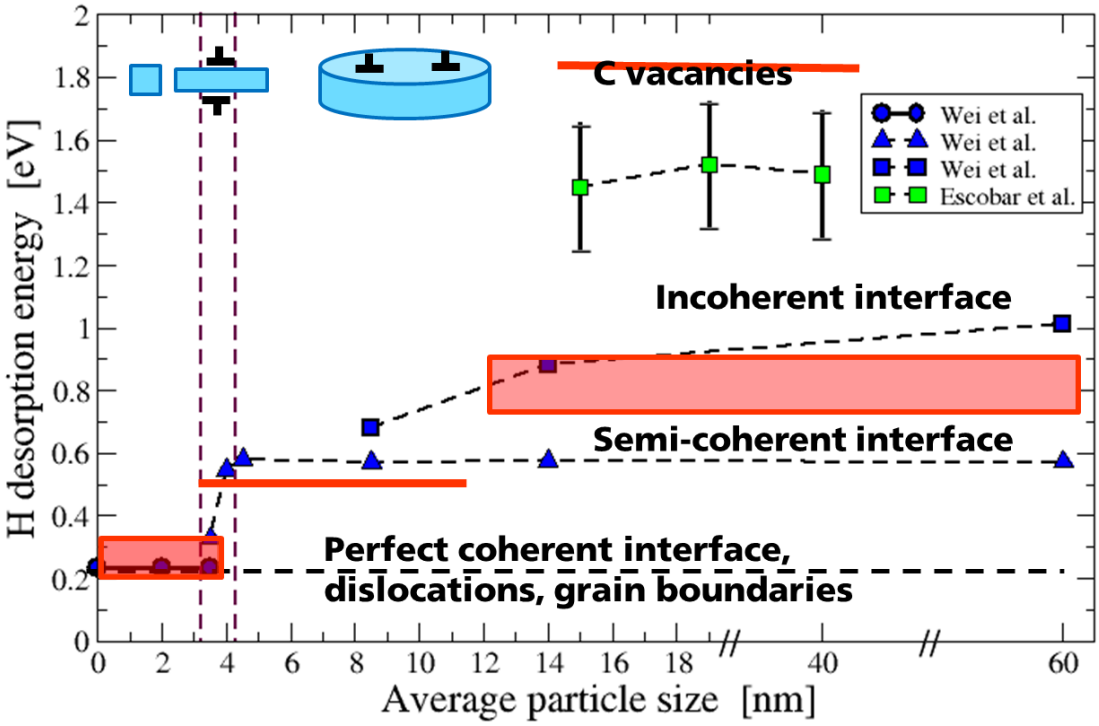

Figure 43: Comparison of calculated and experimental results for H trapping (or desorption) energies as function of TiC particle size. Red lines and dashed areas mark the theoretical results.

Our results show that different particle sizes, interface morphologies, and additional defects, such as vacancies, have a strong influence on H trap energies. Perfect coherent interfaces have very low trapping energies that cannot be distinguished from those of other microstructural defects (dislocations, grain boundaries). Semi-coherent interfaces provide intermediate trapping, mainly by misfit dislocation cores. The trapping at incoherent interfaces depends on a particular atomic structure with a broad range of trapping energies. Carbon vacancies inside the carbide particles act as very strong traps, but they can be occupied only at high temperatures due to a large migration barrier for H to enter TiC. The theoretical results help to interpret and validate experimental measurements and to clarify the atomic mechanisms that drive the observed reduction of diffusible H in steel grades containing finely dispersed carbide particles.

WP4.3: Studies of hydrogen-dislocation interactions in iron

H mobility in metals is strongly affected by line crystal defects – dislocations. Dislocations can serve as trapping sites for H, but they can also enhance H diffusion via so-called pipe diffusion mechanism where H can diffuse more rapidly along the dislocation line than through bulk lattice. In addition, H segregated at dislocations can affect their mobilities as well as mutual elastic interactions. Studies of H-dislocation interactions are therefore very complex and require both reliable and efficient atomistic models to simulate extended atomic ensembles of interacting defects.

The key prerequisite for this study was a development of a reliable model describing the interatomic interactions between Fe and H. The chemical bonding in all bcc transition metals is characterized by strong, unsaturated, directional, covalent bonds originating from the interactions between valence d-electrons and is further complicated by magnetic effects in case of bcc Fe. In order to simulate complex H-dislocation interactions, we developed an advanced magnetic bond order potential (BOP) for the Fe-H system. Since the BOP models are derived by rigorous approximations to the electronic structure methods, they provide a correct description of both the directional covalent bonds and the magnetic interactions in iron. In addition, the BOPs can be applied to significantly larger atomic ensembles than DFT calculations and provide much larger flexibility in the choice of boundary conditions, which is often crucial for obtaining meaningful results in simulations of extended defects. The magnetic BOP for Fe has been shown to correctly predict not only the equilibrium dislocation properties but also the behavior of dislocations under applied stress, both in excellent quantitative agreement with DFT calculations and experimental estimates.

We examined the interaction of interstitial H with both the ½<111> screw and edge dislocations in bcc Fe using the BOP for Fe-H. For the edge dislocation, our calculations show that there is a strong disparity for H interacting with the compressive and tensile regions of the dislocation elastic field. In the compressive region the binding energies are positive, so that H is thermodynamically unstable there and will be repelled from this region, while the H binding energies in the tensile region of the edge dislocation (including the glide plane itself) are strongly negative, meaning a preferential segregation of H atoms in this area. The predicted maximum binding energies of 40-50 kJ/mol correspond to intermediate trapping, similar to that of H in vacancies or grain boundaries. Since the number of favorable interstitial sites on the tensile side is relatively large, the edge and mixed dislocations are likely to significantly affect the H diffusivity. In the case of the screw dislocation, only negative binding energies were found in our calculations, corresponding to favorable segregation of H in the vicinity of the screw core, but the strength of trapping depends sensitively on the H position.

3.5 WP5: KMC calculations and constitutive laws of diffusion

3.5.1 Scope and objectives

The principal remit of WP5 was to provide kinetic Monte Carlo (kMC) calculations leading to a microscopic derivation of diffusion equations that can be fed up into the finite element modelling. Subsidiary goals were (i) to develop an off-lattice kMC model for simulating stress assisted diffusion and trapping of hydrogen by crystalline defects, (ii) to make atomic scale calculations to feed up into the kMC models in conjunction with WP 4, and (iii) to develop a constitutive model for hydrogen with traps.

3.5.2 Summary of results

WP5.1-5.3: Development of off-lattice kMC models describing hydrogen diffusion in defect-free and defective crystals

The principal outcome of this work package is an off-lattice kinetic Monte Carlo model for simulations of diffusion and trapping of atomic hydrogen in the iron lattice with or without crystalline defects. The aim of the kMC simulations was elucidation of the predominant hydrogen transport modes in the presence of typical crystal lattice defects under different initial conditions. Due to the quantum nature of the proton, even at room temperature, the binding energies and energy barriers for diffusion were determined using a tight binding (TB) approximation and Feynman's path integral method. Binding energies and energy barriers from atomistic TB simulations were incorporated to the kMC model as precomputed tables. Hydrogen diffusion and trapping was simulated in the ideal lattice, where obtained results are in agreement with published experimental data. Simulation runs were also performed in the vicinity of typical crystal lattice defects, functioning as trapping sites for hydrogen (vacancies, dislocations and grain boundaries) under conditions of low trap occupancy. Concentrations of H in the simulation box were increased, to account for higher defect densities. Starting conditions were chosen to resemble real microstructures and results obtained from kMC simulations were used for elucidation of the competition between hydrogen trapping at dislocations (see Figure 44), short circuit diffusion along grain boundaries, pipe diffusion along dislocation cores and the influence of microstructural inhomogeneities on hydrogen diffusion. It was found out that effective diffusivity is several magnitudes lower compared to ideal lattice. Comparison between edge and screw dislocations revealed that diffusion of H in the vicinity of a screw dislocation is considerably lower compared to the edge dislocation. Furthermore, pipe diffusion along a dislocation core is lower, compared to the diffusivity near to the dislocation line. Moreover, results obtained from the kMC simulations were put into database of diffusion coefficients for use in numerical simulations, based on finite element methods (FEM). The effective diffusion coefficients in the database are represented as a weighted average of the diffusion coefficients obtained by kMC simulations in different phases and in proximity of typical lattice defects (vacancies, dislocations and grain boundaries). The diffusion coefficients determined by the kMC simulations were included in the anisotropic

diffusivity terms incorporated into the novel constitutive laws which we have developed.

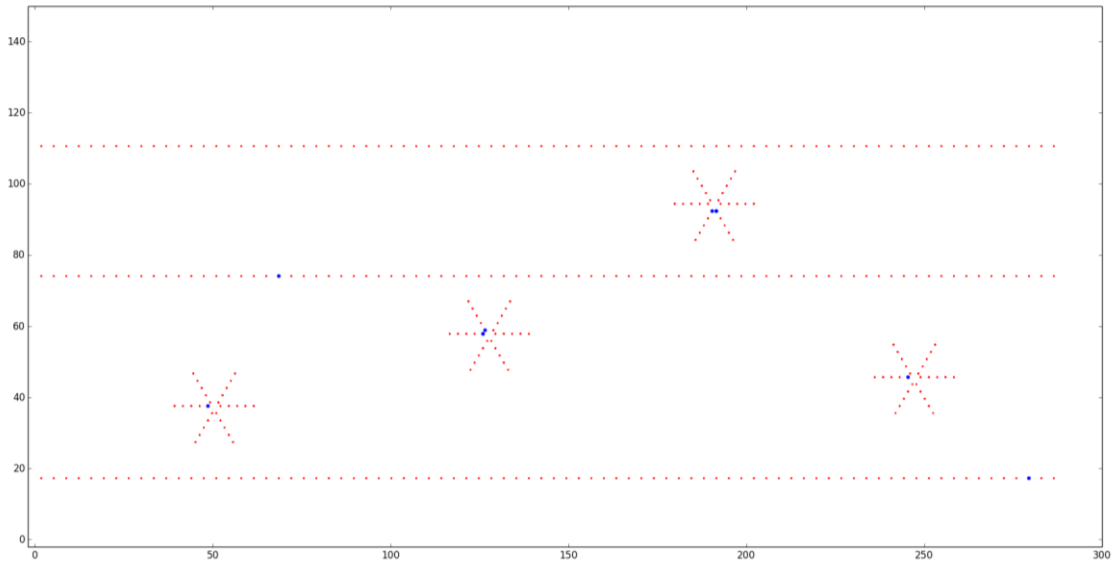

Figure 44: Positions of the H atoms (blue) after 32.175 ms obtained with kMC simulations with combination of ½<111> screw and edge dislocations. Positions of the trap sites generated by the dislocations are depicted as red dots.

WP5.4: Derivation of constitutive laws of diffusion

The main outcomes of this work package have been the derivation of the governing equations and associated boundary conditions for hydrogen transport in crystalline materials, and the development of a software tool to support industrial application of hydrogen transport models based on these equations.

The governing equations are based on conservation of mass and are thermodynamically consistent with the atomistic simulation methods used in the project. The boundary conditions balance the effects of multiple electrochemical and physical processes to correctly evaluate the mass flux of hydrogen at a free surface, a key step forward from the common assumption of constant surface concentration.

The governing equations and boundary conditions have been implemented as a suite of user-defined elements within a proprietary finite element software package, ABAQUS. The use of finite element analysis to solve the equations means that general problems in three dimensions under multi-axial loading can be solved without needing to restrict the problems to simplified geometries. The implementation as user elements in a proprietary package means that large models can be solved in a computationally efficient manner with a small associated software development cost, and that subsequent dissemination (possibly via licensing) of the software will be straightforward. ABAQUS is a commonly-used package for engineering applications, so the potential market for the software is sizeable.

The software implementation has been validated against a simple one-dimensional model of a permeation test. This simple model, in conjunction with the derived boundary condition, has been used to examine the effects of the key experimental parameters (sample thickness and charging current) on permeation test results, leading to a report outlining the optimal conditions for testing. Further support has been given to project partners on developing models of permeation tests and on fitting model results to experimental data.

The software implementation has been disseminated to project partners directly. The work has been promoted to the wider community via a presentation, “Modelling for measurement of corrosion and cracking”, at the NAFEMS World Congress in 2013. NAFEMS is an international organisation promoting good practice in finite element modelling with membership drawn from industry and academia, and its members are ideally placed to benefit from the outcomes of this project as they are already aware of the utility of FE modelling.

3.6 WP6: Continuum and specimen modelling

3.6.1 Scope and objectives

The main goal of WP6 was implementation of the constitutive laws developed in WP5 into finite element (FE) models of H diffusion for our model materials. The FE models were applied to develop an understanding of H-microstructure interactions in the materials, with the aim of identifying key microstructural features and defects that affect the distribution of H. An important part was also determination of the critical conditions corresponding to the onset of damage. This was carried out by calculating the local conditions corresponding to experimentally measured macroscopic thresholds and applying this to a variety of structures. The critical combinations of H concentration and accumulated damage were then incorporated into “scaled-up” component models in WP7 in form of damage criteria.

3.6.2 Summary of results

WP6.1: Continuum modelling

CS1

In CS1 it was apparent that the propagation of cracks was associated with interfaces between grains or grain clusters in PP-Ni (see Figure 45).

Figure 45: Interface crack in PP-Ni.

In order to predict the cracks, a coupled micro-macro scale model was developed using ABAQUS. The macroscale model provided computational efficiency and the microscale model allowed the differential transport of hydrogen to be predicted in areas where cracks were possible. The computational model used the standard ABAQUS mass diffusion model with the addition of extra element types, as developed in WP5, to include the effect of traps in the model. As part of the verification of the model, Voronoi triangulation was used to generate a synthetic microstructure. Figure 46 shows the results from the modelling of a sample with a crack.

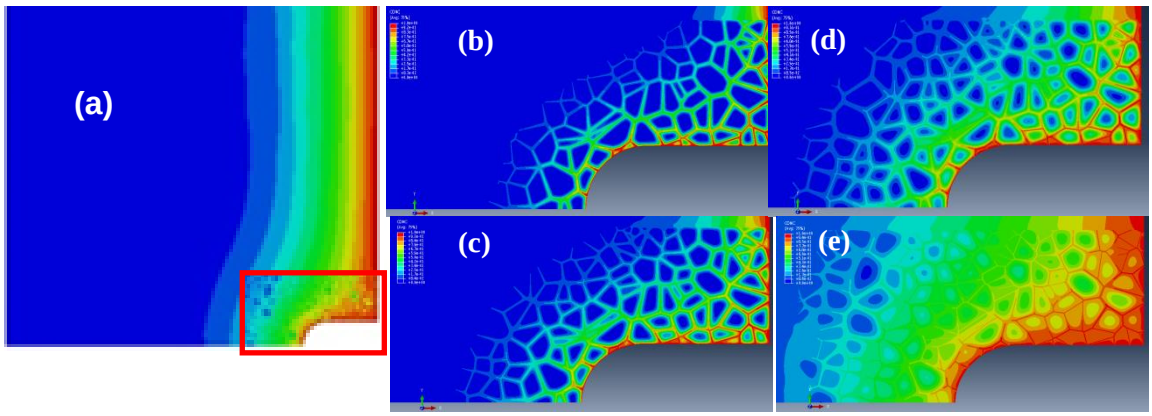

Figure 46: The simulation results of the hydrogen concentration on a coupled two scale model with crack. The complete domain is shown in (a) with concentrations at the end of the simulation. (b) to (e) show hydrogen concentrations at selected time steps

CS2

The continuum modelling for CS2 consisted of two parts. In the first part, the analysis focused on the choice of an appropriate mechanical model (finite strain, elasto-plastic material law) and the corresponding model parameters (hardening law) in order to calculate correctly the stress-strain distributions in test specimens and components. The effect of hydrogen was neglected at this stage.

The main outcome of the second part was a collection of model equations ready for the simulation of stress-strain assisted hydrogen diffusion including trapping effects. The stress-strain fields were assumed to be given from the modelling and the corresponding calculations considered in the first step.

Depending on the features of the measured permeation transients an appropriate set of equations could be selected from the collection of diffusion models. For almost all

model materials in CS2, the model[4] called “stress assisted diffusion with plastic deformations and explicit trapping effects for simple materials” turned out to be sufficient for reproducing the permeation transients. The stress-strain dependence of this model arises from the flux contribution involving the hydrostatic stress and from the trap density expression being a function of the equivalent plastic strain.

CS3

Continuum model of hydrogen diffusion and trapping was developed by the USAL team from discrete random walking principles. Generalised diffusion-trapping equations were derived in this framework. Known special models are retrieved from the proposed one by omission of certain terms that may be small under some circumstances.
The evaluation of H diffusion and trapping in bodies undergoing rolling contact showed only slightly elevated H concentrations may occur in the fatigue process zone. This result is difficult to rationalise with the purported acceleration of fatigue damage processes by absorbed H. Hence, the accumulation of H is largely defined by the equilibrium concentration of H trapped at deformation-induced defects rather than by diffusion driven by stress and/or concentration gradients. This is due to: (i) the short period of time a point on the contact surface spends under load relative to the period of rotation; and (ii) the spatial separation of the hydrostatic and von Mises components of the contact stresses.
Based on these results, it seems reasonable to describe the distribution of H in the near-contact region in terms of the distribution and trapping characteristics of deformation-induced defects. This demands far more rigorous treatment of the hardening behaviour of the material including any microstructural changes that may occur over very large numbers of cycles.

WP6.2: Validation of continuum models

CS1

[4] A.H.M. Krom, R.W.J. Koers, A. Bakker, *Hydrogen transport near a blunting crack tip*, Journal of the mechanics and physics of solids, 47, 1999, pp. 971-992

The coupled model was then validated against experimental results. In this case EBSD scans were used as the starting point for the geometry and mesh used in the validation exercise. The grain boundaries and grain orientation were extracted from the EBSD file. A similar technique to that used in the verification exercise was then used to obtain a microscale mesh with grains, grain boundaries and triple junctions. Figure 47 shows a comparison of experimental measurements and computational results.

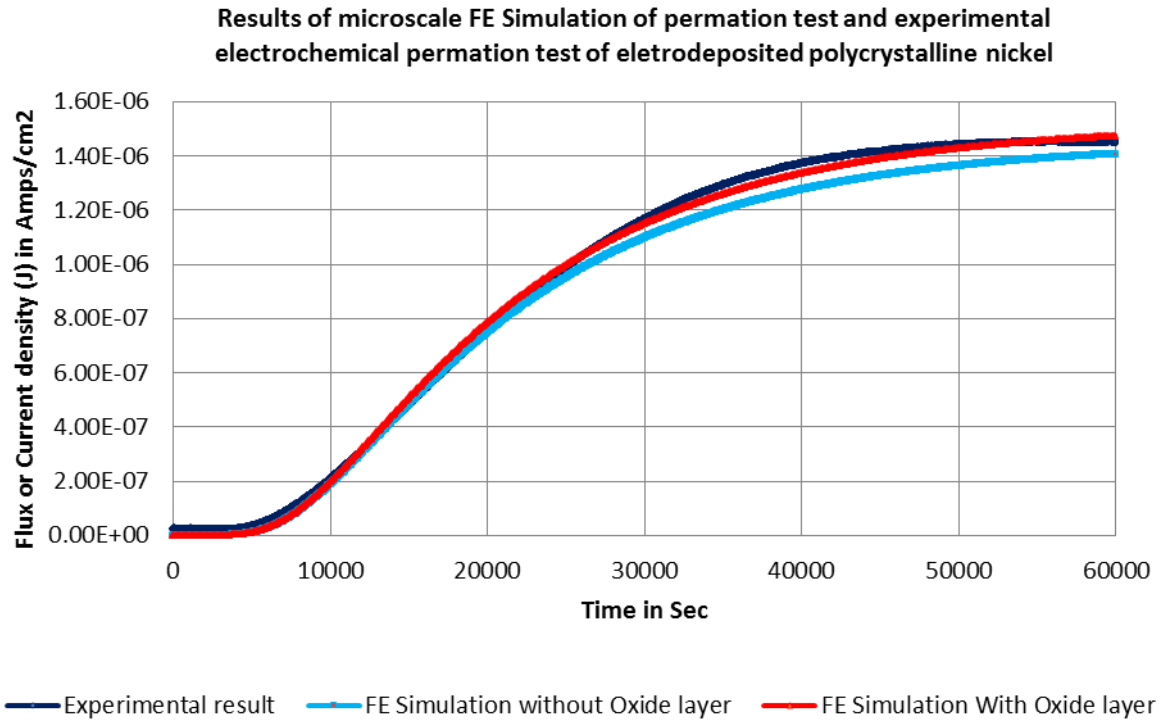

Figure 47: Shows the permeation rate in current density or hydrogen flux of experimentally result and the microstructural finite element permeation simulation with oxide surface layer and without oxide surface layer.

CS2

The H diffusion and trapping parameters for the CP1200 and TKSE concept steels were determined by fitting the experimental permeation curves with a 1D FE model based on the McNabb and Foster equations using a least-squared optimisation algorithm. The correlation between the optimisation solutions was also evaluated. In most cases, the trapping parameters N_1, κ_1 and λ_1 were inherently coupled due to the goodness-of-fit between the measured curves and the analytical solution to Fick's law. Consequently, H diffusivity through these materials could be described in terms of $N_1\kappa_1/\lambda_1$. An exception was the TKSE concept steel 1200M04, for which there was a significant disparity between the measured permeation curves and the analytical solution to Fick's law. This meant that N_1 and κ_1/λ_1 could be evaluated separately.

For the CP1200 samples, the total hydrogen concentrations of the permeation samples were measured using TDS. This enabled the approximation of N_1 and κ_1/λ_1.

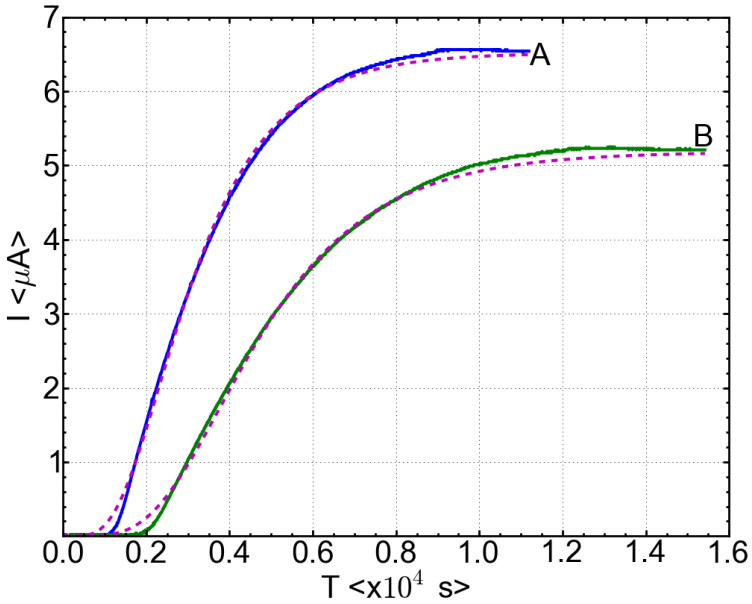

Figure 48: Permeation curves for the Ti-free (A) and Ti-containing (B) 1200M04 model steel. The solid lines denote the measured curves, whereas the dashed lines denote the theoretical curve calculated using the FE model using the optimised values for N_1, κ_1 and λ_1.

CS3

The hydrogen diffusion and trapping parameters for the Grade 7P and Grade 24TM steels in CS3 have also been evaluated using the approach described above. The binding energies of reversible traps in both steels were found to be relatively consistent with those of the TKSE concept steels in CS2. However, the densities of reversible and irreversible traps in the SKF bearing steels are considerably greater than those in the TKSE concept steels. The capture rate constants for irreversible traps for the SKF bearing steels were considerably lower than those for the TKSE concept steels.

WP6.3: Modelling of test specimens

CS1

For determination of fracture criteria, the computational model used diffusion coefficients extracted from the atomistic simulations (WP4). The simulations investigated the effects of the relative orientation of adjacent grains on the stress field and the accumulation of hydrogen. Figure 49 shows the higher accumulation of stresses on a random/general (RGB) grain boundary when compared to a special

(Σ3) GB. This figure shows that the RGBs are likely to have a higher hydrogen accumulation that will increase the probability of crack initiation.

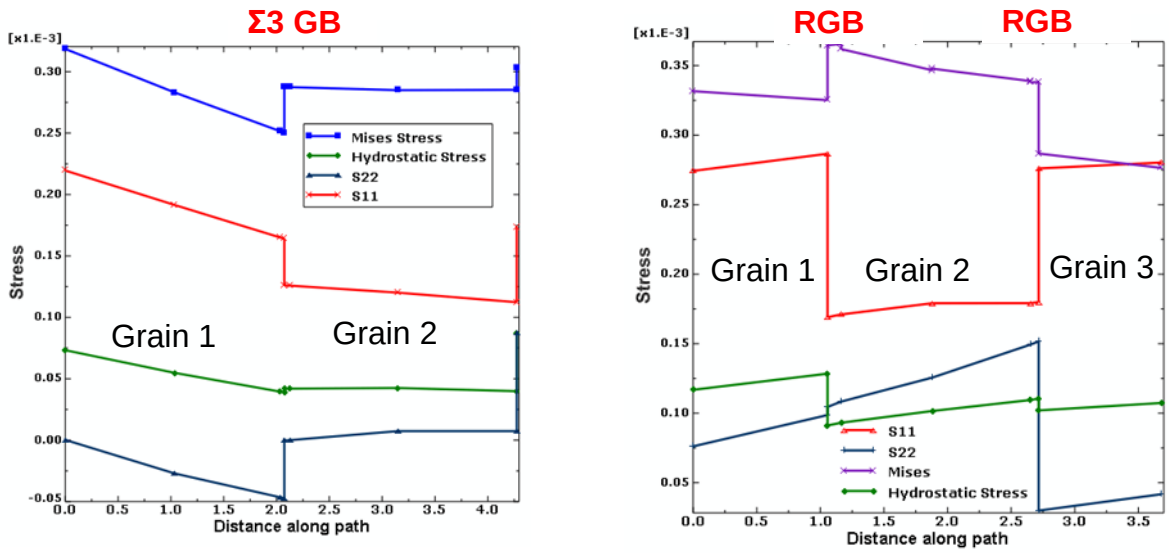

Figure 49: Localised stress distributions along special (Σ3) and random/general (RGB) boundaries.

CS2

The basis for the development of a general fracture criterion for the steels in CS2 was the HE-test introduced by BMW. The main outcome of this test is a graph showing the upper limit of the external load as a function of the total hydrogen content. The measured parameters, however, provide no insight into the local distribution of quantities like stress, plastic strain and lattice hydrogen concentration that are relevant to the fracture criterion. In order to estimate the distribution of these quantities, each test specimen with a critical combination of external load and hydrogen content was simulated with the approach described WP6.1.

The next step in the development of fracture criterion was the introduction of a damage location hypothesis. The analysis of fracture surfaces of ruptured notched specimens motivated the assumption that either the notch tip or the location of the highest hydrostatic stress or the intermediate position between both locations at the mid plane of the specimen is the weakest link and thus the point where a fracture occurs first. Consequently, a critical combination of stress invariants, equivalent plastic strain and hydrogen lattice concentration was calculated for each experiment and possible point of damage initiation. The analysis of the calculated quantities revealed that the von Mises equivalent stress and the hydrogen lattice concentration are the only independent quantities. As a result, the main part of the fracture criterion could be formulated as an empirical function that provides for each value of the von Mises equivalent stress a critical hydrogen concentration above which hydrogen

induced damage likely occurs. Figure 50 shows examples of the critical hydrogen criterion. The comparison of the laboratory grades, for example, clearly illustrates the different resistances against hydrogen induced failure.

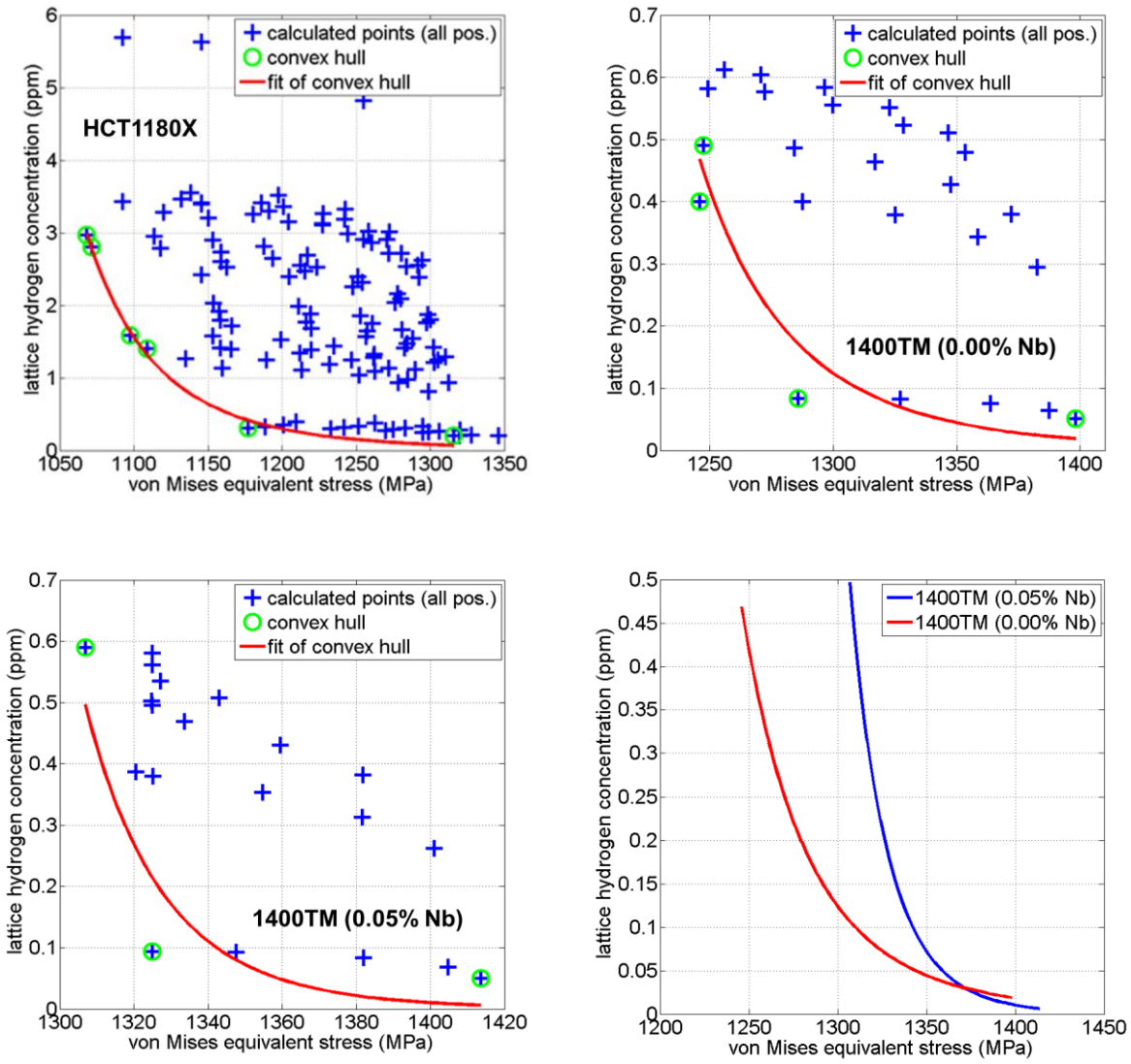

Figure 50: Critical hydrogen concentration criterion (i.e. the function $c^c_L(\sigma_{vM})$) for the commercial grade HCT1180X, the concept steels 1400TM with and without niobium and a comparison of the critical concentrations for the laboratory grades.

The final version of the failure indicator was defined as a probability (0-no risk of failure, 1-high risk of failure) based on the empirical expression for the critical hydrogen concentration. The failure indicator involves the actual hydrogen concentration, the critical hydrogen concentration depending on the equivalent stress, and an expression depending on the hydrostatic stress. The last term helps to

separate regions with tensile stresses from those where the material is under compression. Due to its general form, the failure indicator can be applied to test specimens as well as to realistic components as shown in WP7.

Example simulations of test specimens demonstrated that the risk indicator correctly predicts the effect of reduction of hydrogen content and load level with respect to a critical initial state. Note that the risk indicator includes a safety margin due to uncertainties in the determination of the precise location of the fracture origin in real test specimens.

CS3

In CS3, finite element simulations of hydrogen diffusion in bearings under rolling contact conditions with a constant hydrogen concentration at the contact surface have been performed. These calculations took into account the effect of trapping due to cumulative plastic strain. The model was applied to the simulation of hydrogen diffusion in one of the test specimen geometries used by SKF (see Figure 51).

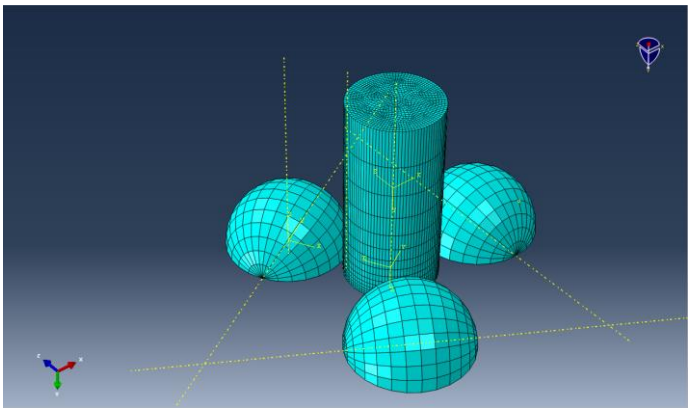

Figure 51: Schematics of the ball-on-rod test.

The calculations were performed assuming isotropic von Mises plasticity model for the rod and elastic behaviour for the balls. Various mesh configurations were designed to achieve the mesh convergence of the solution. It was recognised that to pick up relevant features of stress-strain field, micrometrical scale resolution is required. Concerning the role of friction in rolling contact mechanics, simulations performed for reasonable range of friction coefficient manifest its minor effect on hydrostatic stress field, but rather notable consequences for the cumulative plastic strain distribution.

3.7 WP7: Component modelling

3.7.1 Scope and objectives

The work package contains work that is required to implement the acquired knowledge on hydrogen diffusion in component modelling as it is used by the participating companies, Airbus Defence and Space (formerly EADS), BMW and SKF. What is demonstrated here is that the obtained knowledge is used in the product R&D at the participating companies.

3.7.2 Summary of results

WP7.1: Component modelling

Component modelling for CS1

This case study was concerned with delayed cracking observed on the rocket combustion chamber of rocket engine Vulcain 2, which is the main combustion chamber of Ariane 5 space launcher system. The engine body consists of pulse plated Ni over a Cu substrate, as seen in Figure 52. Cracks are observed to initiate from the heat affected zone, of the weld seam of an Inconel 718 ring on the rocket shell, as shown.

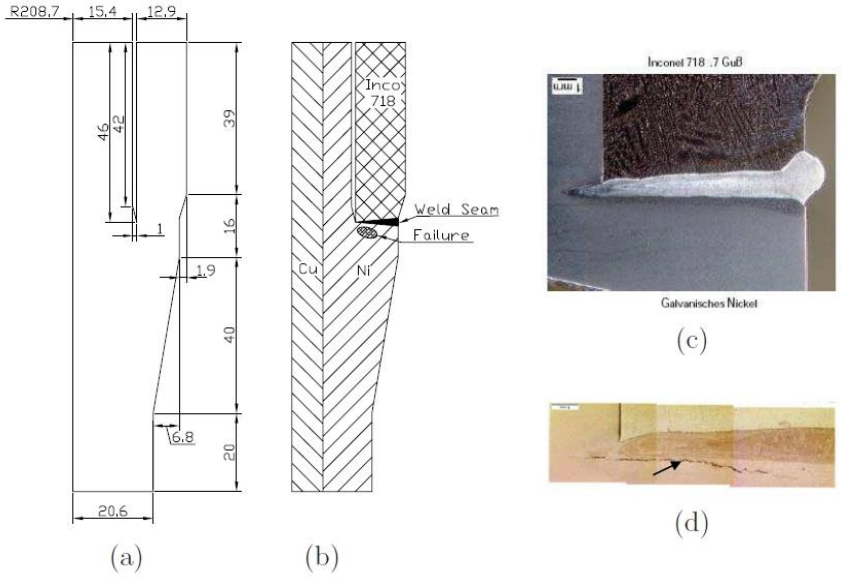

Figure 52: Problem description. (a) geometry, (b) cross section, (c) weld seam, (d) failure.

An ANSYS finite element model of a segment of the rocket combustion chamber was received from Airbus. The model comprised 7 material layers, distributions of hydrostatic stress and plastic strain were provided, as well as the initial concentration distribution and boundary conditions and the concentration state after 3 years of storage.The model was converted for use in ABAQUS and analysed.

The main drivers of diffusion in the ABAQUS model are the initial concentration and the hydrostatic stress field. McNabb and Foster model adds a trap term into the

standard mass conservation equation adopted in ABAQUS, which opens the possibility of incorporating mechanical damage as an additional driver. In order to study the effect of the plastic strain field provided, the McNabb and Foster trap model was implemented such that it could either be run as a user element within ABAQUS, or within an in house standalone FE code.

After verification against the ABAQUS native diffusion element, the new element was used for transient mass diffusion simulations within the rocket combustion chamber segment, for 1095 days. Diffusion parameters used, which were obtained from experimental work and atomistic modelling undertaken in the other work packages.

Various options for the trap model were investigated. The trap density could be assumed to be:

1. constant for an area of interest, such as the heat affected zone,
2. related to the equivalent plastic strain, either by limiting the trap model to the area of damage, or
3. a function of plastic strain according to Sofronis and McMeeking.

The evolution of trap occupation is controlled by probability of capture and release, trap occupancy and local concentration. Figure 53 shows trap site occupation for various trap model options at select milestones for the saturated state, where trap parameters were chosen such that trap sites are allowed to fill up during the simulation period.

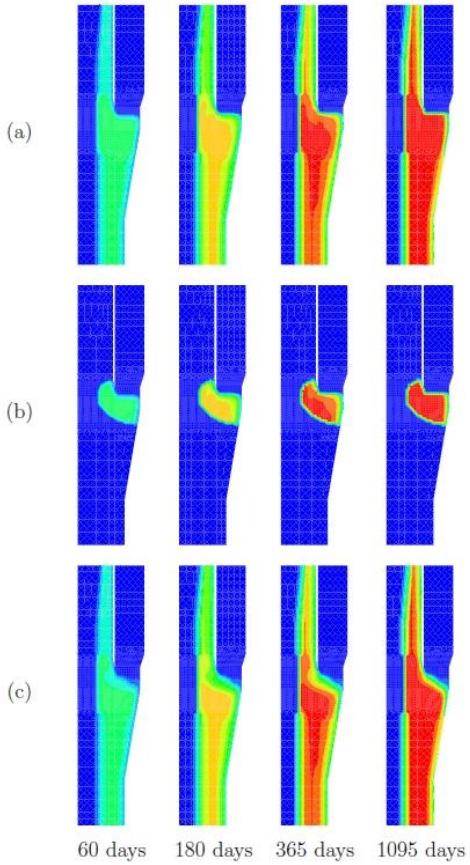

Figure 53: Time history of trap occupation for (a) trapping with constant N_T for the Ni section, (b) trapping with constant N_T for the Ni section with plastic strain and (c) trapping with $N_T=f(\varepsilon_p)$. Blue: no occupancy, red: full occupancy. Initially no occupancy.

Corresponding hydrogen concentration distributions are shown in Figure 54. It could be observed that hydrogen migrates into the weld root and stays there, in very good agreement with the target profile provided. The final H profile is not much different from the standard diffusion model without trapping.

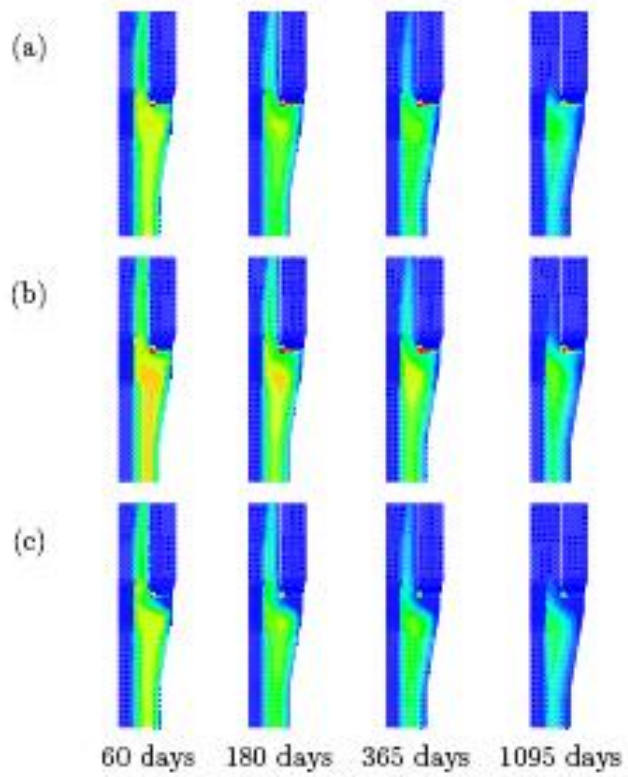

Figure 54: Time history of H concentration for saturated trapping with (a) constant N_T for the Ni section, (b) constant N_T for the Ni section with plastic strain and (c) $N_T = f(\varepsilon_p)$ Blue: 0, red: ≥ 6.5 ppm

Component modelling for CS2

Forming simulations of newly designed components are a standard step during the component development at BMW. An important outcome of these simulations is the distribution of residual stresses and plastic strain in the component after forming. Within MultiHy, a tailored import and data projection approach was developed in order to transfer BMW's 2D simulation data to the 3D COMSOL based simulation framework used for the hydrogen transport simulation and the evaluation of the failure criterion. Figure 55 shows an example of the distribution of the von Mises equivalent stress and the corresponding distribution after the import and projection procedure in a sample component, i.e. an A-Pillar for BMW's 1-series. Both stress distributions and the maximum values are in good agreement, which illustrates the accuracy of the developed approach. Similarly, the distributions of the hydrostatic stress and plastic deformation were transferred to COMSOL. As a result all necessary input data for hydrogen transport simulation and the evaluation of the fracture criterion were available in COMSOL after employing the developed import and projection procedure.

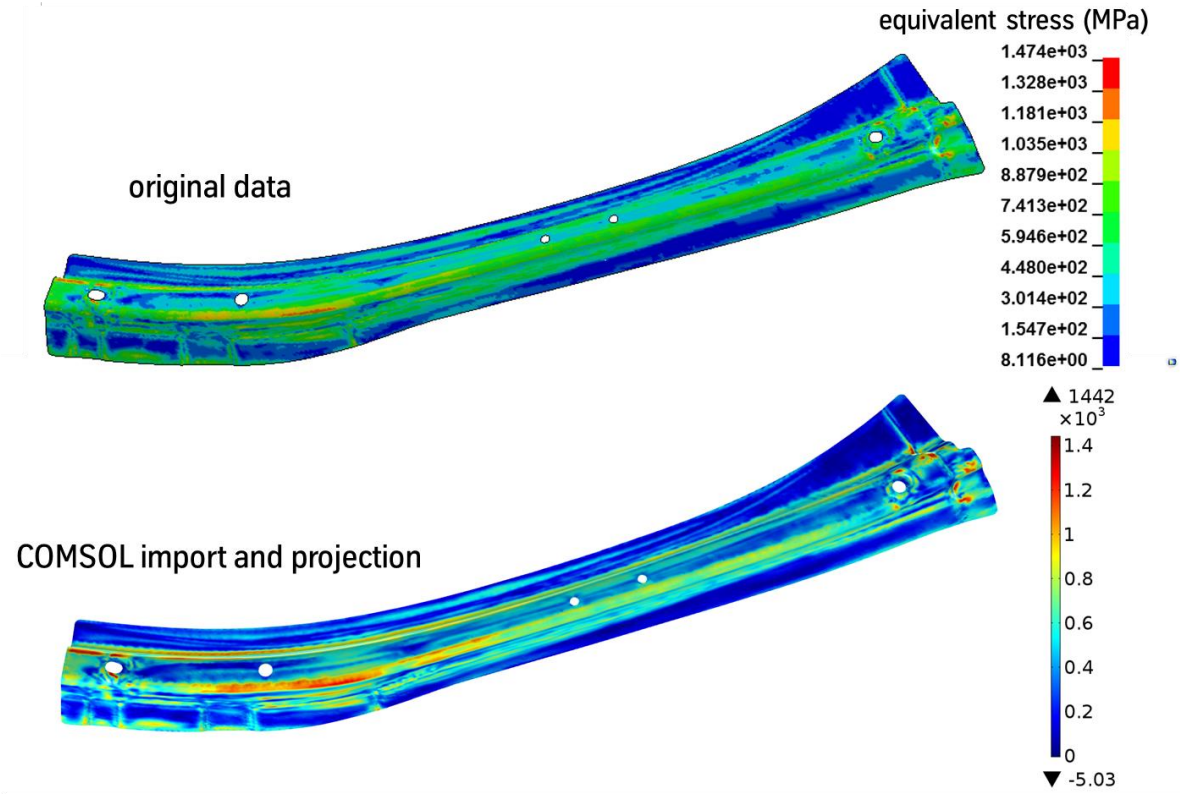

Figure 55: Comparison of the von Mises equivalent stress calculated with BMW's 2D simulation approach and the data after the import and projection procedure in COMSOL.

Based on the imported data, the hydrogen transport model introduced in WP6 enabled simulation of the hydrogen redistribution due to stress, plastic strain and concentration gradients in real components such as BMW's A-Pillar produced from the commercial cold rolled steel HCT1180X.

Figure 56 shows the final results of the transient hydrogen transport simulations with zero flux boundary conditions. While the total hydrogen content of the component remains constant, the uniformly distributed initial hydrogen concentration changes locally according to the hydrostatic stress and plastic strain. As a result, the lattice hydrogen concentration increases or decreases locally by a factor of 2 with respect to the initial concentration. In addition to the final equilibrium concentration, the hydrogen transport simulations also provide insights in the evolution of the local hydrogen concentration with respect to time, thereby enabling calculations of the time to failure.

Another important application of the transient simulations is the incorporation of particular boundary conditions describing, for example, hydrogen effusion or absorption processes in corrosive atmospheres[5]. Transient simulations also enable the consideration of free boundaries with zero hydrogen concentration and arbitrary

[5] A. Turnbull, D.H. Ferriss, H. Anzai; "Modelling of the hydrogen distribution at a crack tip"; Materials Science and Engineering A206 (1996) 1-13

flux. Such edges, created for example by punching, are not coated by a zinc layer such that hydrogen can recombine and effuse from the component. As a result, two competing mechanisms determine the local hydrogen concentration. While the stress-induced hydrogen redistribution may provoke a local increase of the hydrogen concentration, hydrogen effusion through the punched edges leads to a permanent reduction in the hydrogen concentration. Here, transient simulations could be employed to calculate the time to failure that occurs when the local hydrogen concentration exceeds the critical value given by the failure criterion.

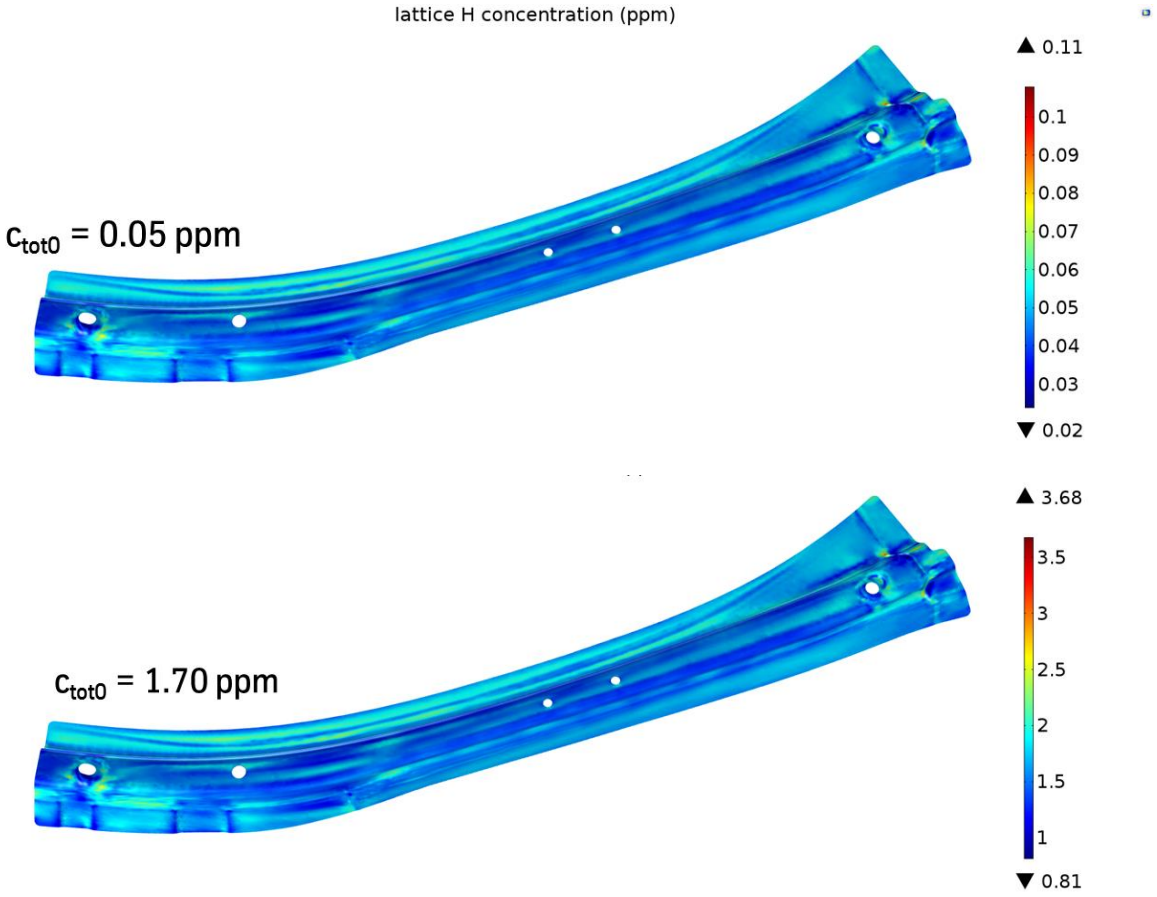

Figure 56: Equilibrium hydrogen lattice concentration for different uniformly distributed initial total hydrogen concentrations (top: 0.05 ppm, bottom 1.70 ppm).

The main objective of the component simulation is the prediction of regions with elevated risk of hydrogen-induced degradation. The tool for this application, the so called ‘failure criterion’, was developed in WP6.

The application of the failure criterion illustrates the effect of different initial total hydrogen contents (0.05 ppm and 1.70 ppm) in the component (A-Pillar) produced from commercial cold rolled steel HCT1180X. In the first case (see Figure 57) the local hydrogen concentration always remains below the critical value and the component is considered safe. In the second case (see Figure 58) the hydrogen

locally exceeds the critical concentration. As a result, the failure criterion assumes values close to 1 which indicates an elevated risk of failure.

Note that the failure criterion can be evaluated in different situations. Since the simulation approach provides the necessary input quantities (equivalent stress and lattice hydrogen concentration) for a wide range of applications, the failure criterion works as a general simulation approach to characterise the risk of hydrogen-assisted component degradation.

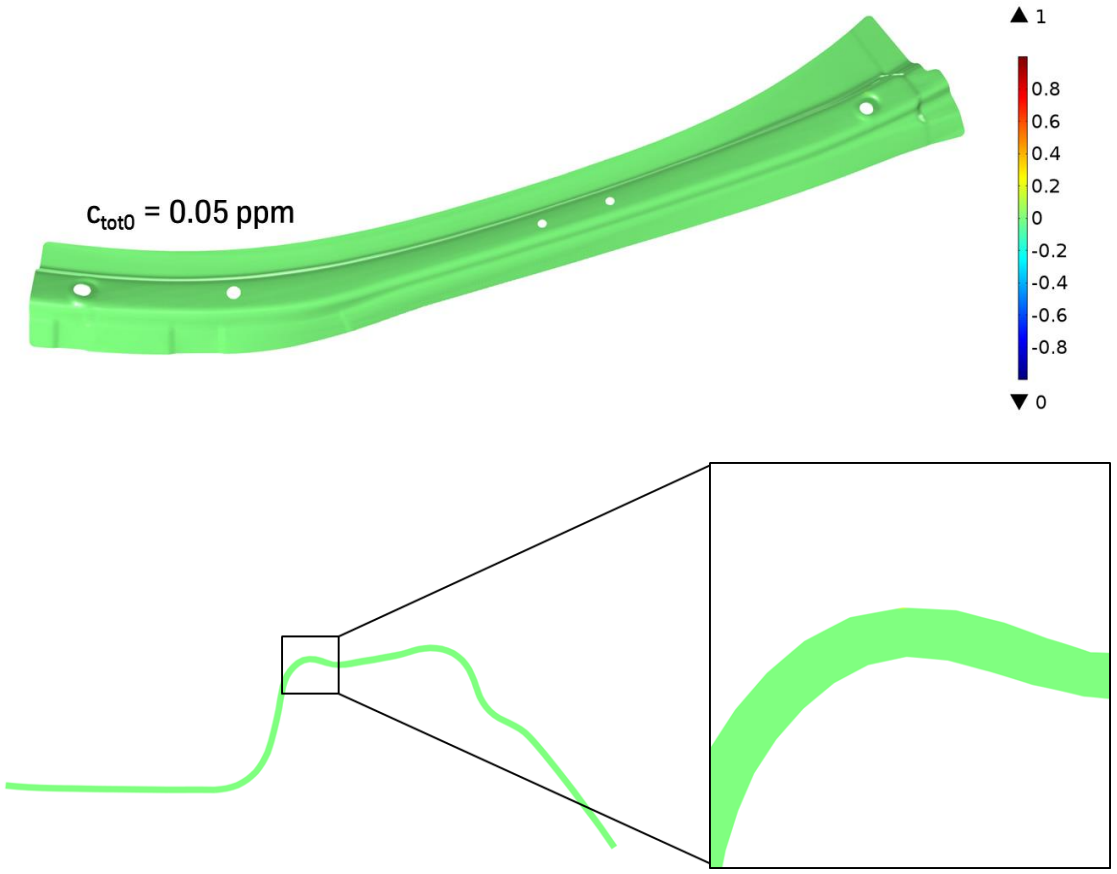

Figure 57: Evaluation of the failure criterion based on the equivalent stress and the equilibrium lattice hydrogen concentration (initial total hydrogen concentration 0.05 ppm).

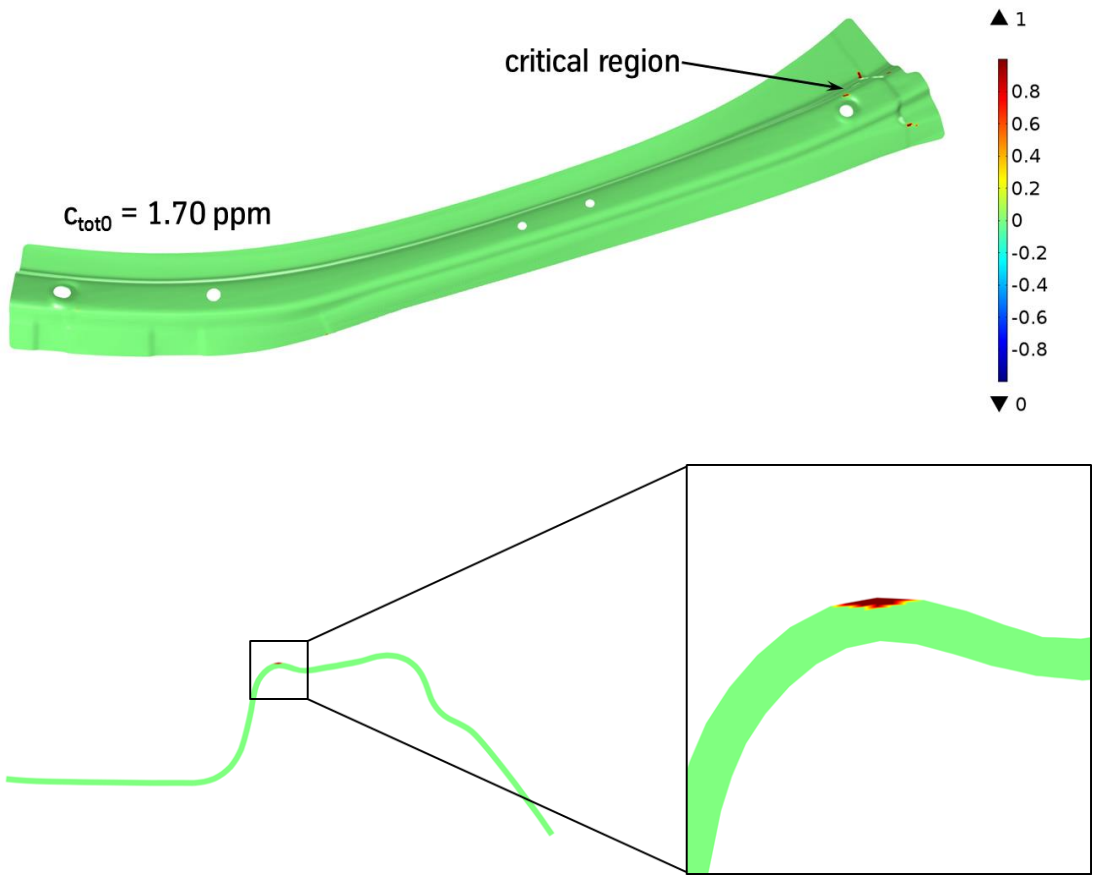

Figure 58: Evaluation of the failure criterion based on the equivalent stress and the equilibrium lattice hydrogen concentration (initial total hydrogen concentration 1.70 ppm).

Component modelling for CS3

The implementation of the developed advanced diffusion model for hydrogen in bearing steel formed the ultimate goal of the project. Several diffusion simulations have been performed to demonstrate the success of this implementation. One example is shown in Figure 59. In this case, a hydrogen concentration at the surface is assumed (for instance hydrogen coming from lubricants) and the distribution during the operation of the bearing is predicted. The example is a Spherical Roller Bearing, but the implementation of the model in generic tools for bearing simulation has given SKF the possibility to get this type of data for all bearing types under all application conditions.

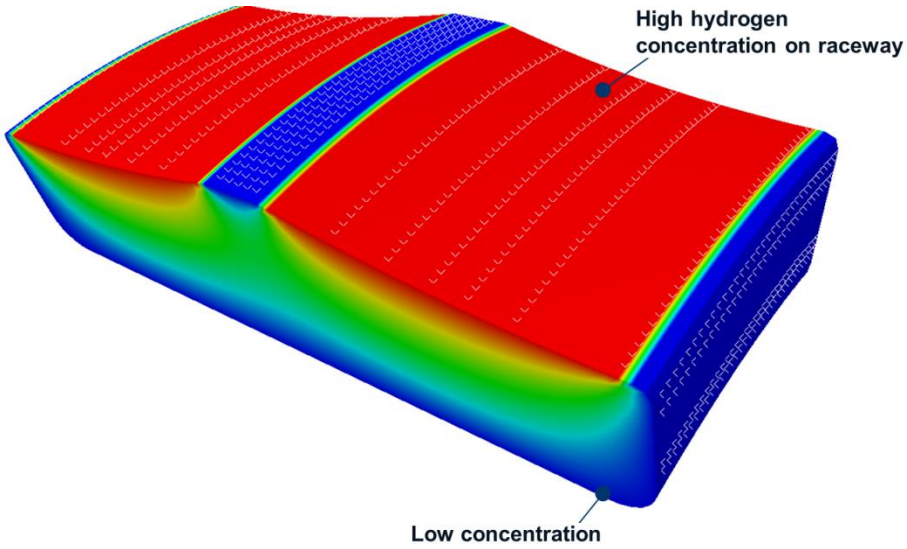

Figure 59 Simulation of hydrogen concentration profile in a Spherical Roller Bearing. An artificial high concentration is put in the simulation to make the gradient visible.

4 Potential impact of project

Hydrogen embrittlement (HE) is a serious and costly industrial problem that affects all structural metals to some extent. Given the ubiquity of hydrogen in service environments, this represents a very serious threat to the integrity of structural components across all industries. HE is an especially important design consideration in the energy, aerospace and automotive industries, where high-strength materials are used and HE-causing environments frequently encountered. The potential consequences of a component failure in these industries include destruction of major infrastructure and loss of lives. Moreover, the continual monitoring, repair and replacement of HE-susceptible components is costly. There is an urgent need to develop a better understanding of this phenomenon, and to develop tools to assist in the design of materials and components for service in HE-causing environments. This would reduce the number of failures in service, thereby increasing safety and reducing material consumption. HE is also one factor preventing the adoption of hydrogen as a widespread replacement for fossil fuels to power automobiles and generate electricity. This is becoming increasingly necessary as legislation aimed at meeting binding targets for emission reduction is introduced in Europe and elsewhere. Currently there is fierce competition between the EU and other nations to set the benchmark in implementing the technology to reduce CO_2 emissions. The development of computation tools to assist in evaluating the compatibility of materials with hydrogen would provide a technological edge in this race and would have a direct impact on CO_2 emissions.

The primary objective of MultiHy was to develop an advanced modelling framework that could be used to predict the HE-susceptibility of real materials and components under actual operating conditions. By focusing on developing accurate descriptions

of H transport and trapping, rather than attempting to model the inherently uncertain H-assisted damage mechanisms, we have developed a robust and transferrable methodology that may be applied to a broad range of industrial problems involving HE. A key aspect of this methodology is the transfer of information pertaining to H-microstructure interactions at the atomistic, meso and macro scales. This information has been acquired through coordinated modelling efforts using a broad range of techniques, including first-principals (i.e. DFT), large-scale molecular dynamics, kinetic Monte Carlo and finite element simulations. Moreover, the models have been informed by data collected from in-service measurements and component testing. An extensive experimental program was also carried out in order to obtain data to validate and supplement the modelling results. The effectiveness of the models has been demonstrated by assisting the industrial project participants in finding solutions to three industrial case studies involving HE. Through their participation in the project, these participants have developed key competencies that will enable them to develop materials, components and production processes that minimise the risk of failure due to HE. This will ultimately help reduce the cost associated with HE-related failures in service.

4.1 Use of project outcomes in CS1

Maintaining the reliability and increasing the cost effectiveness of space vehicles and infrastructure are of the utmost importance to the future of the European space program. One way of achieving these goals is to introduce materials with enhanced functionality and reduced production costs. Due to the harsh conditions encountered in space applications, the demands placed on such materials are extreme. They must fulfil strict rules in order to be considered fit-for-service and the margin between safe operation and failure is often thin. Thus, optimisation of material properties and the production chain is imperative.

Pulse plated (PP) Ni is used in the fabrication of critical components for the Ariane 5 satellite delivery vehicle. While most electroplating processes use a direct current (DC), pulse plating processes use an alternating current with a very high current density. This results in a better surface finish, which in turn reduces production costs by eliminating the need for subsequent machining. PP-Ni materials are also stronger than to DC-Ni materials, thereby enabling the fabrication of thinner, and therefore lighter, components. This ultimately has an influence on the fuel efficiency and payload capacity of the vehicle.

During the pulse plating process H is produced and may be absorbed by the deposited metal. After deposition the components undergo further machining and joining processes, which result in residual stresses. Depending on the plating parameters used, the combination of H and residual stresses may be sufficient to cause cracking. This may occur after the component has been in storage for a period of time ranging from days to years. Whilst this does not pose an immediate structural integrity problem, it does highlight the need to better understand the influence of microstructure and process parameters on the susceptibility of PP-Ni to HE.

The financial losses associated with such failures are enormous. Due to the strict qualification requirements, failure in one component would result in the entire batch

being rejected. The later the failure occurs, the higher the economic loss. The worst case scenario – besides the failure occurring during operation of the launcher – would be if the technical failure is realised at the moment when the system being prepared for launch. This would require the launch to be aborted, resulting in a financial loss of several million Euros.

The potential cost of technical failures necessitates the thorough inspection of all components in order to detect problems at the earliest possible stage. It also means that processes used in the manufacture of critical components are optimised so that the structural integrity of critical components can be relied on. In order to achieve the required level of dependency, it is necessary not only to optimize materials and processes through experimental procedures, but also to complement this by simulation of the manufacturing processes and their influence on material behaviour right up to the moment of operation of the combustion chamber.

Grain boundaries may have a strong influence on H diffusion in polycrystalline materials. For f.c.c. materials such as Ni, for which the rate of H diffusion between normal interstitial sites is relatively low, grain boundaries may act as preferential diffusion pathways. This may have a significant influence on the overall H diffusion rate in fine-grained or nanocrystalline materials. PP-Ni microstructures may be comprised of grains ranging in size from <5nm to >10µm. Indeed, the results of electrochemical permeation testing in MultiHy showed that H diffusion through PP-Ni is slightly faster than that in pure Ni, suggesting that the contribution of grain boundary diffusion to the overall H diffusion rate was significant. Thus, a key focus of MultiHy has been evaluating the H diffusion and trapping characteristics of various types of grain boundaries in Ni and the influence of different grain structures on the macroscopic H diffusion rate.

At the atomic level, both first-principles and large-scale molecular dynamics simulations were used to evaluate the energy barriers and binding energies of H atoms in and around grain boundaries in Ni. This data was used in kinetic Monte Carlo simulations of idealised grain structures in order to evaluate the influence of grain size and connectivity on the effective H diffusivity. Various finite element (FE) modelling routines were used to evaluate long-range H diffusion, taking into account both grain boundary and bulk diffusion, in PP-Ni. These were based on meshes generated from microstructural data collected using electron backscatter diffraction (EBSD). These models were scaled-up to simulate H diffusion in a multi-material component containing pre-existing defects.

The outcomes of the MultiHy project have already been utilized in numerous activities related to launcher development and production at Airbus. The simulation tools were used to validate the assumption that delayed cracking of PP-Ni components – such as the load bearing nickel jacket for the VULCAIN 2 combustion chamber - is a consequence of H absorbed during the electroplating process. Furthermore, H diffusion towards the weld seams due to large welding stresses was simulated for the anticipated lifetime (up to 6 years) of the combustion chamber. Based on this, the qualification process for VULCAIN2 was finally implemented in the manufacturing chain, resulting in cost and lead time reduction.

Extending this approach, the prediction of weld stress levels during the development phase for a given material with defined H content and diffusivities is now feasible. This allows the design of weld seams (or other elements inducing local stress peaks) avoiding the risk of H embrittlement in an electroformed Ni-shell. The simulation tools may also be used for assessing the reaction of H sensitive materials to an H environment.

Prior to the MultiHy project, an assessment of a space components' susceptibility to HE was not or only partially feasible. The newly developed tools are now implemented in the material development routines and in some cases even in the production control. Due to this, Airbus was able to make a decision upon the material for the recently developed combustion chamber of Ariane 6 upper stage motor - VINCI. Before, this selection could only be made after a series of dedicated tests on full-scale components at a very late stage of the motor development. Even though the analysis and assessment procedure for HE is currently restricted to the electroplating process and related materials, an extension to other materials is in preparation.

4.2 Use of project outcomes in CS2

There is a growing interest in the use of advanced high strength steel (AHSS) grades for structural automobile components as a means of improving fuel economy through lightweight construction whilst still meeting stringent safety standards. AHSS have the potential to withstand higher stresses than normal steels, thereby enabling the design of structural components with thinner sections, while maintaining high ductility, which is necessary for energy absorption during a collision. However, these properties can be degraded by H, which may be absorbed as a result of production or manufacturing processes (e.g. casting, annealing, coating, forming or joining), or during the component lifecycle (e.g. as a result of corrosion). The relatively high susceptibility of AHSSs to HE is a major barrier to their widespread use in the automotive sector. It is widely assumed that the HE susceptibility of metals increases with their tensile strength. Though this may be a crude generalisation, it highlights the growing need to better understand HE as the average strength of steels used as structural automobile components increases. At present, the use of AHSSs in service is generally limited to those with tensile strengths <1000 MPa. Though higher strength steels exist, they are excluded from use in critical structural components due to concerns over HE. There is strong demand from automobile manufacturers such as BMW and steel suppliers such as TKSE and VAS for computational tools to: (i) assist in qualifying AHSSs for service and establishing appropriate design limits; (ii) determine the impact of different production processes on the structural integrity of components; (iii) simulate the diffusion of residual H due to local stress fields in components during manufacturing; and (iv) to assist in improving the HE resistance of steels by microstructural modification.

Steel is one of the most important materials for modern economies. It can be adjusted to achieve a wide range of physical properties, is relatively cheap and easily processed and has a wide range of applications. Steel can also play a crucial role in

mitigating the climate change process. The use of innovative steel products and processes (e.g. in the automotive and construction industries, for pipelines or in the energy sector) can lead to a considerable reduction of CO2 emissions. A 2007 study by the Boston Consulting Group [6] showed that the German steel industry alone generates 67 Mt of CO_2 annually. The potential for CO_2 reduction through to the application of innovative steel products is 74 Mt annually, of which 11.2 Mt can be achieved by weight saving solutions in car bodies, e.g. by the use of AHSS grades. These estimates are very conservative; the potential of reduction of CO_2 emissions may be 2-5 times higher. Therefore, the use of innovative steel products and production processes will play an essential role in meeting the EU's CO_2 emissions targets.

The reduction of CO_2 emissions is one of the main driving forces behind the development and application of new materials in today's automotive industry. It has been estimated that by reducing the overall weight of a car by 100 kg, the average fuel consumption and CO_2 emission for that car would be reduced by 0.3 – 0.5 L/100km and 7.5-12.5 g/km of CO_2 (or 1.8 t of CO_2 annually) respectively. Given that the total number of cars in the EU is 187 mil [7], the potential for reducing CO_2 emission by component weight reduction is enormous. The use of innovative alloys (e.g. AHSS grades), processes (e.g. the hot forming process), semi-finished products (e.g. tailored Blanks or tubes), or complex component solutions (e.g. the advanced door concept within the InCar® project) can result in a component weight reduction of 10 - 30 % [6,8].

AHSSs are seen as a particularly promising means of reducing the weight of automobile chassis components. The component weight reductions achievable through the use of AHSSs are comparable to those achievable using Al alloys; however, the total energy required for producing a steel component is several times less than for producing the same component from Al. This is in an important factor affecting of the sustainability of the entire automobile production chain. In addition to reducing the overall weight of automobiles, AHSSs also have the potential to improve occupant safety. AHSSs can withstand higher stresses than ordinary steels and, therefore, give the passenger compartment cell better resistance against deformation and intrusions during a collision. This reduces the risk of severe injuries or death of the occupants. Moreover, certain AHSSs have greater ductility than ordinary steels, so they can absorb more energy during a collision. By enabling the design of thinner structural elements, AHSSs also give the driver an increased field of vision, thereby increasing safety for pedestrians and other motorists. AHSSs already constitute 60 % of the weight of some compact cars (e.g. Fiat 500, Opel Corsa or Ford Ka) [7];

---

[6] CO_2 Bilanz Stahl, The Boston Consulting Group, Stahl-Zentrum, Düsseldorf, 2010

[7] Faszination Stahl, *Schlankheitskur*, Stahl-Informations-Zentrum, Düsseldorf, 2008, p7

[8] InCar® – Der innovative Lösungsbaukasten für die Automobilindustrie, ThyssenKrupp AG, Düsseldorf, 2009

however, extending their application to other vehicle classes requires a solution to some environmentally-assisted degradation issues, in particular HE.

AHSSs, especially high-manganese steels or dual- or complex-phase steels, are highly susceptible to HE. This susceptibility is accentuated by production processes that introduce H and residual stresses into the material. H absorption occurs during hot forming, which takes place during the steel production cycle, and during joining and plating processes, which are carried out during component manufacture. The use of Al or Zn based coatings for corrosion prevention also increases the risk of HE by acting as a strong barrier against effusion (i.e. by trapping the H inside the component). The combination of absorbed H and stresses applied during component fabrication, assembly and service can result in failure of the component during the production process or slow degradation of the structural integrity of the component during service. Therefore, the use of such steels for automobile components requires a detailed understanding of the amount of H introduced during the production cycle and its ability to cause damage.

With current technology, the evaluation of the HE-susceptibility of complex steels must be carried out largely in the laboratory using experimental techniques. This process is extremely time and manpower intensive. An integrated modelling tool to evaluate the HE-susceptibility of materials and components would minimise the demand on costly experimental work and help reduce the-time-to-market for new steel grades. The development of new steel grades is essential to the reduction of greenhouse gas emissions in line with EC targets.

The steel industry is a vital part of the European economy and provides employment for more than 400,000 EU residents. In recent years, the industry has come under increasing pressure from non-European steel producers, in particular from the availability of low-cost commoditized grades from Chinese steel producers. The European automotive industry, which employs some 2.2 mil EU citizens directly (plus 9.8 mil indirectly) [9], has also come under considerable pressure from non-European competitors in recent years. The availability of an integrated modelling tool to evaluate the HE susceptibility of materials and components would provide these industries with a technological advantage over their non-EU competitors, thereby benefitting the EU as a whole.

In addition to the development of numerical tools to predict the susceptibility of AHSS components to HE, there is also a need to develop strategies to improve their resistance to HE through microstructural characterisation. One possible means of achieving this is by reducing the rate with which H accumulates at crack initiation sites by introducing strong, innocuous trap sites to the microstructure. TiC and NbC particles are have long been known to behave as strong trap sites. Thus, the primary focus of CS2 was the evaluation of the H trapping characteristics of TiC and NbC particles and their influence on the HE susceptibility of AHSS grades. For that

---

[9] European Automobile Manufacturers Association, 2008, http://www.acea.be/images/uploads/files/20081003_Pocket_Guide.pdf

purpose, two model steel compositions, the “TKSE concept” and “VAS concept”, were developed in MultiHy. The TKSE and VAS concept steels were fabricated with and without Ti and Nb respectively using laboratory-scale casting, rolling and annealing equipment. Microstructural characterisation of the materials later revealed that the VAS concept steels did not contain pure NbC particles. Thus, subsequent work focused wholly on evaluating the influences of TiC particles.

First-principles calculations were used in CS2 to evaluate the H trapping properties of TiC particles. The H trapping properties of TiC particles were also evaluated experimentally using thermal desorption spectroscopy (TDS) and electrochemical permeation testing. The susceptibilities of the TKSE concept steels to HE were evaluated by constant load testing of H-charged samples. The data obtained from atomistic calculations and experiments was used in FE simulations of H diffusion in the constant load samples as well as in real “body in white” components. The simulations of H diffusion in the constant load samples were used to determine the stress/strain condition and H concentration at the point and instant of fracture. These results were then incorporated into the component models as fracture criteria.

The FE modelling in CS2 has been performed entirely by industrial partners. These partners now have a robust methodology, which combined experimental and theoretical analysis of H diffusion and H-assisted fracture, that may be applied to the evaluation of real components to HE. This will ultimately enable them to assess the susceptibility of AHSS components to HE before the component is fabricated.

Due to the promising results of the MultiHy project, the notched tensile test was accepted as a first HE-test in the BMW homologating process of AHSS grades with a tensile strength above 1000 MPa. At the moment this HE-test is being evaluated in the VDA (Verein Deutscher Automobilhersteller) for HE in order to become a standardized HE-test.

The project has also advanced our collective understanding of H trapping mechanisms in steels and their influence on HE susceptibility. A key outcome of the atomistic modelling and experimental work was that TiC particles act as H traps, but the addition of Ti to AHSS grades also results in a considerable reduction in grain size. Both effects influence H diffusion at room temperature, since grain boundaries may also act as H traps. Overall, the investigations validated the positive impact of Ti-microalloying on the HE-resistance and confirmed the increase in HE-resistance with increasing yield ratio. This knowledge along with the knowledge gathered from microstructure evaluations will help to develop new steel grades with higher HE-resistance. This will strengthen the position of European steel suppliers as innovative product developers.

4.3 Use of project outcomes in CS3

Wind energy is becoming an increasingly important source of clean energy. It will play a crucial role in achieving the EU’s target of a 20% reduction in greenhouse gas emissions due to primary energy production by 2020 (relative to 1990 levels). It has been estimated that a single wind turbine can save 5,000 tons of CO_2 over its lifetime

[10]. Unlike fossil fuels, the application of wind energy will not be limited by unavailability of the resource, but rather by the economic and environmental factors. Wind turbines have a high “visual impact” and are a significant contributor to noise pollution, particularly in urban environments. One means of overcoming these factors is placing wind farms offshore. It is expected that the next generation of windmills (10 MW or higher) will be situated mostly at off-shore sites.

Offshore wind turbines also have the advantage of being able to produce more energy, since the size of the turbine is not limited (e.g. by road transportation or noise regulations) and the average wind speed over open water is generally higher than over land. However, offshore wind turbines are inherently more expensive due to practical difficulties associated with installation and maintenance. The positioning of turbines offshore also introduces new technical challenges that are related to the harsh environments in which they operate. Among these is the greater propensity for HA-RCF. This can be attributed to either: (i) the use of long-life lubricants containing a high number of additives; and (ii) the increased likelihood of moisture entering the bearing. Long-life lubricants contain certain additives due to the long maintenance intervals, but are more prone to decomposition and H generation. At the same time the salty environment increases the corrosion related damages and hence the probability of H penetration into the component. The consequences of failure in a critical component (e.g. the rotor or gearbox bearing) in terms of financial costs, waste material, and greenhouse gas emissions, are considerable. Thus, developing a better understanding the causes of H-related failures is a critical step towards making wind energy a viable solution to the world’s energy problems.

Given the size of bearings used in wind turbines, and the logistical challenges associated with their installation and maintenance, the financial and environmental cost of wind turbine bearing failure is very high. Consequently, there is great demand for modelling tools to assist in predicting H-related failure of bearing components based on real microstructural and environmental information and to develop ways of mitigating this problem, e.g. by microstructural modification.

There is a need to better understand the role of different microstructural features in HA-RCF and to quantify their influence on the service life of bearing components. By better understanding the role of microstructure in the mechanism for HA-RCF, it is possible to develop ways to mitigate the effects of HA-RCF, e.g. through microstructural modification. The availability of modelling tools to predict HA-RCF will also assist the development of innovative, energy-saving bearing designs. New bearings designs have the potential of decreasing rolling resistance by as much as 30% in applications where power consumption exceeds 1 MW. This would result in less energy loss and higher power output. It has been estimated that replacing a bearing in a typical 2MW wind turbine with the new, more efficient design, would result in an energy saving of 2.6 million kWh per annum. If the bearings in all of the world’s wind turbines could be replaced with this new design, they would generate an

---

[10] Energy Efficient Solutions, SKF, http://www.skf.com/files/876508.pdf

extra 770 million kWh a year [11]. That is equivalent to the total energy consumption of 1 million Swedish households for one month. Such gains could be achieved by optimisation of the bearing materials and geometry. An optimised bearing is lighter, which itself is more energy efficient because it takes less power to move the rolling elements. It also lowers inertia of the moving parts thus reducing the chance of skidding and smearing, which would otherwise affect performance and service life. However, changes to the microstructure or geometry can have unforeseen consequences on degradation and reliability. In order to avoid these, a profound understanding of the complex relationships between the material, lubricant and contact loads and their impact on HA-RCF is required.

An understanding of the influence of H on the mechanisms for degradation and reliability of wind turbine bearings can also be applied to wind turbine operation logging and telemetry. The most modern wind farms use condition monitoring systems to collect, store, transmit and analyse system data (e.g. bearing vibration), allowing the operators to monitor the performance of the turbines and carry out risk analysis remotely. The software enables maintenance activities to be planned pro-actively, thereby extending the time between site visits (difficult and expensive in the case of offshore installations) and reducing the risk of unplanned downtime. This capability would be enhanced if condition monitoring software could consider the influence of H on bearing integrity. This would give operators the ability to predict H-related failures before they occur, further reducing downtime and losses in energy output.

The MultiHy project has given SKF many benefits in terms of knowledge development. The project was hosted by the central research facility of SKF, the Engineering & Research Centre. In the project, a study has been made on the physical behaviour of hydrogen in bearing steel using advanced tools such as diffusion measurements using the Devanathan cell and Thermal Desorption Spectroscopy. This has led to an increased understanding of the relation between materials used by SKF in its products and hydrogen.

Similarly to CS2, one of the main topics of CS3 was the evaluation of the H trapping characteristics of carbides, in particular VC particles. These have already been shown by SKF to have a positive influence on the resistance of bearing steels to HA-RCF. First-principles calculations of H trapping by VC particles were performed by SKF with the support of Fraunhofer IWM. This has given SKF the ability to investigate the influence of microstructure on the H diffusion and trapping properties of bearing steels, and ultimately their susceptibility to HA-RCF. The results of the atomistic calculations have also been used in FE simulations of H diffusion under rolling contact conditions in a broad range of bearing geometries. This has yielded a number of insights into the mechanisms for HA-RCF that will, ultimately, enable SKF to better predict the influence of H on the lifetimes of bearings in service.

---

[11] Press statement, 06.03.2007: “SKF presents new Energy Efficient bearings saving at least 30% energy consumption”, http://www.skf.com/skf/news/html

In order to analyse the measured data, special software was developed with support of NPL, one of the other partners in the project. This software, based on genetic algorithms, allows the user to generate input data for complex hydrogen diffusion simulations from measured diffusion curves. This made a big impact on the analysis time in the laboratory and allows the SKF laboratories to generate much more sophisticated parameter sets for diffusion simulations.

Ultimately, the result of the project is being implemented in bearing simulation tools. This will make a wide application of the knowledge acquired in the MultiHy project possible for all bearing types and operational conditions. With this, SKF will gain a competitive advantage in the market when it comes to applications where hydrogen influences bearing material and thereby bearing performance.

The execution of the project has also been beneficial for SKF as it has increased the competence level of SKF researchers in this field.